Addis Ababa University
Addis Ababa Institute of Technology
School of Civil and Environmental Engineering

Post Graduate Studies in Geodesy and Geomatics

A gravimetric method to determine horizontal stress field due to flow in the mantle in East Africa Great Rift Valley

BY:

Abenezer Getinet

GSR/5947/12

Advisor:

Dr. Andinet Ashagire

A Thesis Submitted to the School of Post-Graduate Studies of Civil and Environmental Engineering, Addis Ababa University, in Partial Fulfillment of the Degree of Master of Science in Geodesy and Geomatics

July, 2023

Addis Ababa, Ethiopia

Approval Sheet

Addis Ababa University

Addis Ababa Institute of Technology (AAiT)

School of Civil and Environmental Engineering

The undersigned have examined the thesis entitled "**A gravimetric method to determine horizontal stress field due to flow in the mantle in the East Africa Great Rift Valley**" presented by **Abenezer Getinet**, a candidate for the **degree of master of Science in Geodesy and Geomatics** and hereby certify that it is worthy of acceptance.

Dr. Andinet Ashagire		14/07/2023
Advisor	Signature	Date
Sintayehu A.		13/07/2023
Internal Examiner	Signature	Date
Ephrem Yadeta		12/07/2023
External Examiner	Signature	Date
Abrham Gebre (Dr.) Dean, School of Civil & Environmental Engineering		
Chair Person	Signature	Date

Declaration

Addis Ababa University

Addis Ababa Institute of Technology (AAiT)

School of Civil and Environmental Engineering

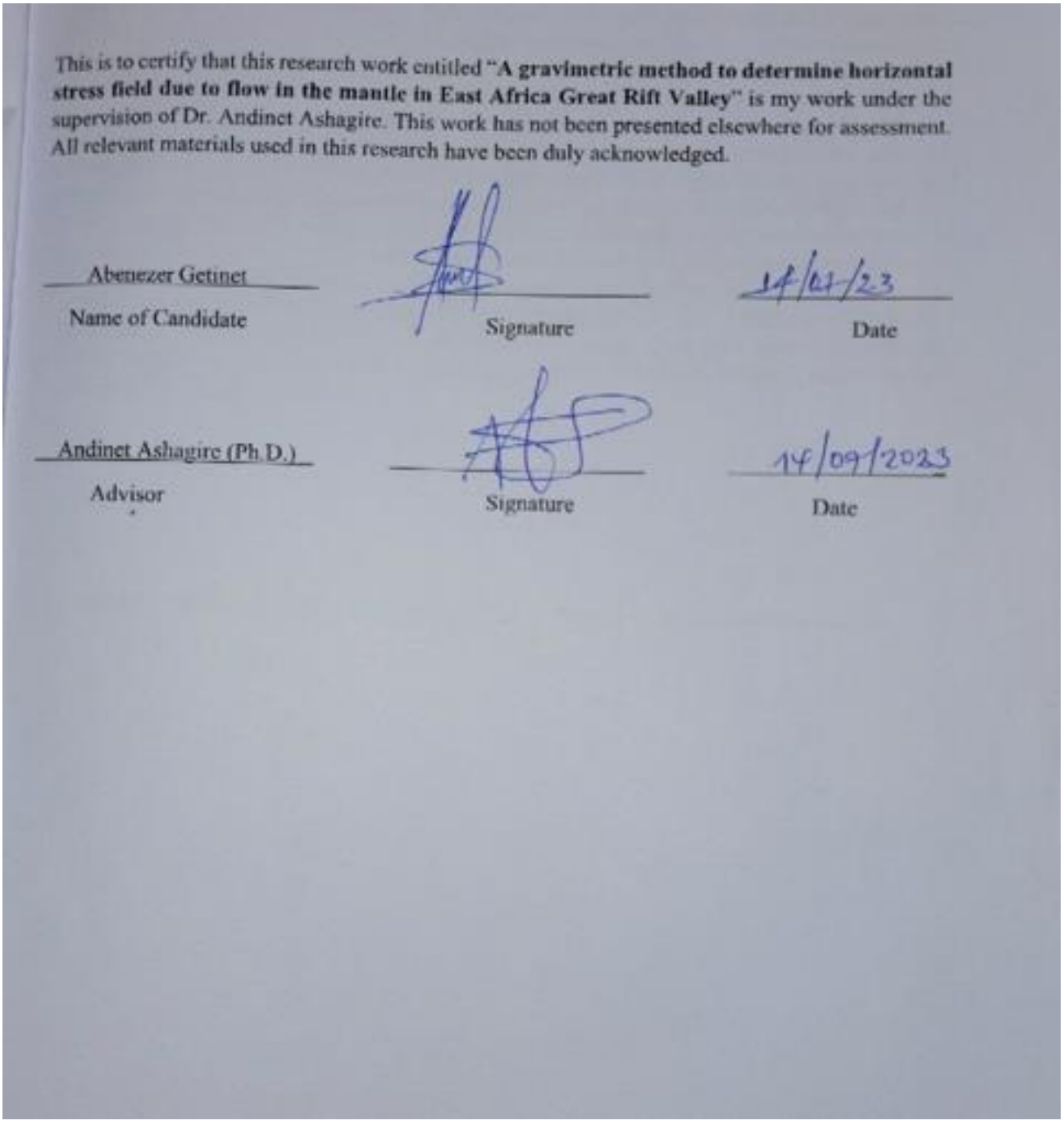

This is to certify that this research work entitled "**A gravimetric method to determine horizontal stress field due to flow in the mantle in East Africa Great Rift Valley**" is my work under the supervision of Dr. Andinet Ashagire. This work has not been presented elsewhere for assessment. All relevant materials used in this research have been duly acknowledged.

Abenezer Getinet — Name of Candidate

Signature

14/01/23 — Date

Andinet Ashagire (Ph.D.) — Advisor

Signature

14/09/2023 — Date

Abstract

The gravimetric approach has been widely used to determine the stress field of subsurface geology of the earth crust. Mainly this study aimed to determine lithospheric shear stress in the Earth's mantle and its temporal changes caused by geodynamical movements. The gravimetric approach is applied, to evaluate the stress at the base of lithosphere and to detect changes in stress using static gravity field model EGM08 and GRACE monthly solutions respectively. In addition to the static gravity field data some physical information about topographic height, crustal thickness, and lithospheric thickness are incorporated in this method. As a result, more geophysical information and data are applied for computation of horizontal lithospheric stress in this approach. To do so, depth of the base of lithosphere determined by subtracting topographic height from lithospheric thickness is needed, thus the lithospheric shear stress component computed at the base of lithosphere. Moreover, the comparison of lithospheric shear stress using different static gravity field models are performed. The estimated horizontal shear stress at the base of the lithosphere throughout the study area revealed 55.68% of the stress is oriented in a northward direction and the remaining 44.32% is oriented in the southward direction; 44.41% of the stress is oriented in an eastward direction and the remaining 55.59% is oriented in the westward direction: and the result of the estimated horizontal shear stress magnitude ranges from ≈ 0.04 MPa to ≈ 15.32 MPa. Furthermore, the estimated horizontal shear stress components show good agreement with the tectonic boundaries and the location of stress regimes in the WSM2016 database, as well as the seismic events in the study area.

Key words: lithospheric stress, gravimetric, GRACE, static gravity field, mantel convection

Acknowledgments

Words cannot express my gratitude to my advisor Dr. Andinet Ashagire for his invaluable patience, guidance, support and feedback throughout my master's program. I also could not have undertaken this journey without my advisor, who generously provided encouragement, knowledge and expertise invaluable to me and have played a crucial role in the success to complete this research and write this thesis.

I am grateful to Dire Dawa University for providing me an award to study master of science program at Addis Ababa University. I am also grateful to Addis Ababa Institute of Technology (AAiT), School of Civil and Environmental Engineering for providing me with the opportunity to conduct my research and for their financial support they provided. I am indebted with thank Girum Ashenafi, who went beyond to help me with my research work.

Lastly, I would be remiss in not mentioning my parent, especially my mother Abebayehu Gashu, her belief in me has kept my spirits and motivation high during this process. Without her encouragement and motivation, I would not have been able to complete this journey.

Table of Contents

List of Figures

List of Tables

List of Acronymous

ACC	SuperSTAR Accelerometer
BDS	BeiDou Navigation Satellite System
CHAMP	Challenging Minisatellite Payload
CSR	Center for Space Research
DDK	Denoising and Decorrelation Kernel
DEM	Digital Elevation Model
D-InSAR	Differential Interferometric Synthetic Aperture Radar
DOWR	Dual One Way Ranging
EARS	East African Rift System
EGM	Earth Gravitational Model
EIGEN	European Improved Gravity model of the Earth by New techniques
GFZ	GeoforschungsZentrum Potsdam/ German Research Centre for Geosciences
GIA	Glacial Isostatic Adjustment
GNSS	Global Navigation Satellite Systems
GOCE	Gravity field and Steady-State Ocean Circulation Explorer
GPS	Global Positioning System
GRACE	Gravity Recovery and Climate Experiment
GRACE-FO	Gravity Recovery and Climate Experiment Follow-on
ICGEM	International Centre for Global Earth Model
IGFS	International Gravity Field Service
ITG	Institute of Theoretical Geodesy
InSAR	Interferometric Synthetic Aperture Radar
JPL	Jet Propulsion Laboratory
KBR	K-Band Ranging
LRI	Laser Ranging Interferometer

NGDC	National Geophysical Data Center
NOAA	National Oceanic and Atmospheric Administration
NASA	National Aeronautics and Space Administration
SAR	Synthetic Aperture Radar
SDS	Science Data System
SGD	Satellite Gradiometry Data
SGG	Satellite Gravity Gradiometer
SLR	Satellite Laser Ranging
SRTM	Shuttle Radar Topography Mission
SST	Satellite-to-Satellite Tracking
VLBI	Very Long Baseline Interferometry
VMM	Vening Meinesz–Moritz
WSM	World Stress Map

CHAPTER ONE

1. Introduction

1.1 Background of the Study

According to M. D. Zoback and Zoback (2002), stress is a tensor that represents the density of forces operating on every surface passing through a point. To understand the dynamics of tectonic processes, earthquakes, and earth surface deformation monitoring, it is essential to study stress fields. The crust, mantle, outer core, and inner core are the four concentric shells that make up the Earth. As a result, the depths, volumes, and densities of various strata vary. Densities, however, change laterally and with depth. The volumes vary, and the mantle's volume is unusually vast compared to the volumes of the other layers. According to (Bagherbandi, 2011), the Earth's crust, mantle, outer core, and inner core make up 2%, 80%, 17%, and 1% of its total volume, respectively. The lithosphere of the Earth floats on the mantle, and the convection process inside the mantle strains the lithosphere and produces plate movements. This stress is directly related to the mantle convection pattern, viscosity, and the lithosphere and mantle's physical and geometrical features (Eshagh, 2017). Studying the sub-lithospheric stress created by mantle convection is critical for monitoring tectonics, comprehending seismicity and volcanicity, and investigating subsurface geological information that is used for a variety of real-world applications (Liu, 1977). Being sympathetically aware of the forces that drive and oppose plate movements, the mechanics of seismic and aseismic faulting, and the rheology of the crust and upper mantle, requires knowledge of the level of stress in the lithosphere. Our understanding of dynamical processes in the Earth's subsurface and on its surface over geologically long periods is necessary to simulate the manifestations of intraplate stresses (Lithgow-bertelloni & Guynn, 2004).

The main causes of stress are active tectonic flow in the mantle, heterogeneities in the density of the crust and the mantle, the load of isostatically uncompensated topographic features on the crust, crustal flexure, and thermal stresses, according to several earlier studies (M. L. Zoback & Zoback, 1980). The relevant sources of stress can be found at many length scales, from variations in crustal thickness and topography to mantle movement at the global level. At a much lower length scale, sedimentary basins and complex fault systems that are linked to rapid spatial variations in stress regimes can be detected. The global tectonic stress field and its alterations are strongly related to the driving force underlying plate tectonics. Mantle sources can also be limited as a function of time by looking at how they affect other geological and geophysical observables, such as plate velocities, subduction histories, and continental flooding occurrences. For a comprehensive knowledge of the lithospheric stress field at all scales, physical models of fault initiation and lithospheric processes, as well as in-depth investigations of the geology and structural history of particular provinces, are all required (Lithgow-bertelloni & Guynn, 2004).

The estimation of sub-lithospheric stress due to mantle convection is a demanding task or situation and a valuable issue for the geoscience community. Extracting sub-surface information from seismic and gravity measurements is a fundamental task. Since the Earth's gravity field is a

reflection of its internal structure, changes in the gravity field also affect the sub-lithospheric tension and stress that is transmitted throughout the lithosphere. In the meantime, analysis of gravity field measurements is important to calculate sub-lithospheric stresses, such as those caused by mantle convection, which is crucial for geophysical interpretation and evaluation of seismicity, volcanism, kimberlite magmatism, mine stability, underground waste containment, ore concentration, and magnetic and tectonic features (Liu, 1977). In addition, lithosphere stresses are crucial to many geological processes. For geological events as varied as the distribution of earthquakes, the creation of sedimentary basins, and the distribution of fluid reservoirs, the current state of lithospheric stress and its recent evolution are crucial (Lithgow-bertelloni & Guynn, 2004).

Even though the Earth is dynamic, its gravitational field is not stationary throughout time. Large earthquakes and hydrological signals are the main sources that have an impact on the gravity field's long-wavelength structure, among other variables. Due to the high altitude of satellites above the Earth's surface, which reduces the high frequencies of the gravitational field, satellite gravimetry is an appropriate method for these objectives. The kind of satellite sensor, in addition to the satellite's height, is crucial for regaining the gravity field (Eshagh, 2021). Satellite gradiometry is more useful for retrieving high frequencies of the gravity field than for determining its temporal variations. However, with inter-satellite low-low tracking, when GRACE data are collected from twin satellites orbiting the Earth at the same time, the situation is different since the data collected provide exact information on the low-frequency content of the gravity field and its temporal variations. However, when we apply this supposition to real-world geophysical issues, instruments or sensors sensitive to all gravitational frequency bands are not yet available (Eshagh, 2021). In the meantime, theoretically, any satellite gravimetry data should be able to be used to determine these temporal variations. Due to sensor error characteristics, mission geometry, and perhaps due to restrictions in existing analysis methodologies and background models, these unconstrained GRACE/GRACE-FO monthly data cannot be used to their full spectrum extent without modification (Han et al., 2005). To lessen the consequences of errors in the short wavelength components of the gravity fields generated by the Gravity Recovery and Climate Experiment satellite mission, smoothing is thus necessary. Therefore, a critical mathematical formulation to disclose it should have used a well-known integral representation of equations.

There is no one best way to calculate mantle convection patterns or stresses directly using only gravity data. Different hypotheses have been adopted depending on the study to model the mantle's convection pattern, estimate those sub-lithospheric stresses in geophysics, and understand the causal relationship between mantle convection and geodynamical phenomena like tectonics based on the measured gravimetric quantity. This is because better modeling of the mantle leads to a better determination of the lithospheric stresses.

A map of the lithosphere's state of stress was attempted in early research between the 1960s and 1900s using earthquake focal mechanisms and scanty, often shallow, in situ stress data. However, because there was a relatively low density of stress data in this early research, it was assumed that stresses were homogeneous at a large scale. This was followed by the introduction of an integrated stress mapping technique that took into account a range of geology and geophysical data, including current geologic information on fault slip and volcanic alignments, in situ stress measurements,

stress-induced wellbore breakouts, and drilling-induced tensile fractures (M. L. Zoback & Zoback, 2009).

Furthermore, a vast amount of knowledge regarding the Earth has been supplied in a way that is consistent with the advancement of satellite technology, Earth observation systems, and remote sensing. In comparison to the first-generation global gravity field models derived from the 1960s to 1990s, it is now possible to represent the Earth's global gravity field and its variations with better spatial and temporal resolutions thanks to the highly accurate satellite measurements made possible by today's developing technology. Global gravity models include details on the Earth's mass shift, interior and fluid envelope, and shape, which can help identify changes in the Earth caused by stress. As a result, there have been numerous geodynamic studies undertaken all over the world that examine the level of stress in the lithosphere. For instance, (Runcorn, 1964, 1967) simplifies the Navier-Stokes equations to determine the northwards and southwards subcrustal stress components. The fact that this stress directly links the mantle convection to the Earth's gravity field was discovered by him as the first individual to make the connection between this stress and the gravity information. Using the formulas from (Runcorn, 1967), (Liu, 1977) modeled the convection pattern and stress system beneath the African plate, and (Liu, 1978) did the same beneath Asia. Later, (Liu, 1979) developed a hypothesis relating seismogenic models for the Tangshan Earthquake to the concentration of subcrustal stress. The stresses predicted in the regional compensation scheme are an order of magnitude more than those corresponding to the local one, according to (McNutt, 1980), who used the regional gravity field to examine the stress in the crust and upper mantle. (Huang & Fu, 1982) investigated the tectonic force sources and convection patterns in China. Additionally, using an elastic earth model and solutions to the elastic equations in spheres, (Fu & Huang, 1983) computed the stress pattern globally for harmonics of $2^{o} – 30^{o}$ and used the gravitational harmonics derived from satellite data to model the global stress fields in the lithosphere. (Ricard et al., 1984) examining the connection between the geoid height and the lithospheric stress. He claims that given a homogeneous mass, the surface stress and the geoid height increase with the depth of the perturbing heterogeneity but rapidly decrease beyond a depth that is proportional to the wavelength. In an effort to match the observed intraplate stress patterns computed using a set of 3D global finite element models that included mantle flow, lithospheric heterogeneity, and topography with one specified by the World Stress Map (WSM), the cause of the current level of lithospheric stress is the subject of a detailed investigation by (Lithgow-bertelloni & Guynn, 2004). They looked at two different interpretations of lithospheric heterogeneity, one directly based on seismic and other constraints (Crust 2.0), and the other using a straightforward isostatic compensation model. Additionally, they computed mantle tractions using two models of mantle density heterogeneity. These are based on the history of subduction during the previous 180 million years, one of which is inferred from seismic tomography and successfully reproduces the present-day geoid and Cenozoic plate velocities.

The (Runcorn, 1967) formulas were developed by (Eshagh, 2014) in a way that makes it simple to calculate the sub-crustal stress using satellite gradiometry data (SGD). He used two techniques to create the stress components. First, by introducing some integral estimation techniques to supply the stress components and integrate the SGD. The second way is by creating an integral equation for the SGD's inversion to the aforementioned values. (Eshagh, 2015) discovered the Vening

Meinesz-Moritz theory's mathematical illustration of the relationship that exists between sub-crustal stress and a gravimetrically calculated Moho model. He created three distinct mathematical relationships between the stress components and the global and local Moho models. Later, (Eshagh & Tenzer, 2015) used this technique to determine sub-crustal stress in some regions of the world with unique geophysical characteristics. After analyzing the results, they proposed a new technique for computing the horizontal components of sub-crustal stress based on using the stress function with numerical differentiation to increase the spectral resolution (i.e., the (Runcorn, 1967) method had a limited spectral resolution up to degree 25 of spherical). Research on Iran, (Eshagh & Romeshkani, 2015) used GOCE gradiometric data directly rather than gravity models to derive sub-lithospheric stress resulting from mantle convection. They then immediately inverted those data to the sub-lithospheric stress. A hypothesis for sub-lithospheric stress recovery based on gravity theories was provided by (Eshagh et al., 2016). They created new integral equations and solved them locally across the Indo-Pak (India-Pakistan) area in a way that produced a gravimetric Moho model using a different method. This allowed them to reconstruct the function. They first use data from the SRTM (Shuttle Radar Topography Mission) and the Earth gravity model EGM2008, then use data from the SRTM and the seismic Moho model of CRUST1.0, and finally use data and measurements from the GOCE (Gravity field and steady-state Ocean Circulation Explorer) mission.

(Eshagh et al., 2020) calculated the stress, strain, and displacement inside the lithosphere using the GRACE-FO monthly solutions. They computed the partial differential elasticity equation for the lithosphere while taking into account that it is a spherical elastic shell. They also discovered a unique solution to the elasticity boundary value issue that offers a stable answer. This theoretical model is realistically employed to estimate the stress-strain redistribution induced by earthquakes in Iran. They also use constants of the solution to predict the strain and displacements contributing to these stresses.

Gravimetric modeling was used by (Gido et al., 2018) to simulate a horizontal stress field brought on by mantle flow. They provided a model of sub-lithosphere horizontal stress in the mantle of the Earth and its temporal change related to geodynamical motions such as mantle convection. They employed the Earth's crustal thickness, isostatic models, and GRACE data, respectively, to calculate the sub-lithosphere stress and its temporal fluctuation. They additionally employed the absolute and secular rates of the Earth's gravity field.

Currently, the determination and analysis of sub-lithospheric stress rely on data from the Gravity Recovery and Climate Experiment (GRACE) and GRACE Follow-On (GRACE-FO) gravity-dedicated satellite missions. These missions provide information about the static gravity field as well as, critically, its spatiotemporal variations (Eshagh et al., 2020). The most frequent outputs released by three distinct processing facilities, namely the Jet Propulsion Laboratory (JPL), Center for Space Research at the University of Texas at Austin (CSR), and GeoforschungsZentrum Potsdam (GFZ), are GRACE/GRACE-FO monthly gravity solutions. Due to the numerous parameter options and solution techniques that are feasible, the data appear in three separate processing centers. GFZ, CSR, and JPL each uniquely examine various solution strategies. A set of spherical harmonic coefficients of the "geopotential" is present in the GRACE and GRACE-FO

Level-2 gravity field data packages. The term "geopotential" describes the Earth system's external potential gravity field, which encompasses all of its solid and fluid (including oceans and atmosphere) components. Due to mass movement and interchange between the parts of the Earth system, the geopotential at a specific site changes throughout time (Cooley & Landerer, 2020). To simulate the stress events brought on by mantle movement in the sub-lithosphere at a different time, monthly temporal data is employed.

This research focuses on the lithospheric shear stress and its temporal changes caused by mantle convection in East Africa's Great Rift Valley, also known as the East Africa Rift System (hereafter EARS in this paper), which is studied using static gravity data and GRACE data via a gravimetric approach by developing a mathematical model for describing stress propagation in the sub-lithosphere.

1.2 Statement of the Problem

Determining lithospheric stress has been intensively investigated as an intriguing field of earth system science. The goals have usually ranged from mapping the level of stress in the lithosphere to numerous separate areas of interest that improve understanding of the earth's subsurface geological, geophysical, and geodynamical processes.

The narrow elongate zones of thinned lithosphere associated with deep asthenosphere intrusions in the upper mantle that alter the state of stress in the EARS are the most distinctive features of the rift system (Chorowicz, 2005). This concealed component of the rift structure is indicated on the surface by the thermal uplift of shoulders and supported by geophysical data, but there aren't enough geophysical data to correctly map the stress in these thinned lithosphere zones. Also, diverse geodynamical processes such as mantle convection and horizontal and vertical land motion owing to plate tectonics occur in the EARS. Furthermore, the thermal and dynamic consequences of mantle plumes acting at (or near) the base of the lithosphere are associated with a wide region of anomalously high topography that characterizes the southern and eastern portions of the African continent within the EARS; geophysical and geochemical data support this hypothesis, though no consensus exists concerning the location, depth extent, and continuity of the upwelling hot mantle material (Corti, 2012). These incidents will be responsible for the present state of stress in the area. However, separating and distinguishing gravity signals caused by convection in the mantle and land movements will be a difficult endeavor, and there is also the issue of the degree of extension sustained by the rift system. This means that greater information regarding the condition of lithospheric stress, along with large-scale regional compilations of horizontal lithospheric stress and temporal variations of stress owing to mantle movement across a vast region including East Africa's Great Rift Valley, would be extremely valuable.

To solve all of these difficulties, more in-depth examination utilizing many types of advanced methodologies with up-to-date and accurate data is required owing to the earth's complicated geophysical and geodynamical character. In general, earlier research described in section 1.1 offered a range of methods to solve this problem and assess the lithosphere's stress. Results, however, indicate that it is challenging to establish a coherent stress pattern; this is especially true in the EARS. There has not been enough research done in the East African Great Rift Valley to evaluate the lithospheric shear stress and look into its temporal change, though. So, this study

incorporates this issue and points at a target to provide up-to-date information on the state of horizontal shear stress and the secular trend associated with mantle convection at the base of the lithosphere in the study area and introduce a mathematical model in spherical coordinates for describing it. It is performed by a method that combines, the static gravity field in the spherical harmonic domain through Runcorn's method to estimate the horizontal shear stress components induced by mantle convection and assess the rate of its temporal change by taking advantage of GRACE data using a gravimetric approach at the base of the lithosphere in East Africa's Great Rift Valley. To deal with the noise in the GRACE monthly gravity data, this study adopts a non-isotropic smoothing approach (Kusche et al., 2009). This smoothing technique reduces the effects of errors present in short wavelength components, as discussed in section 1.1, on the gravity fields produced by the GRACE satellite mission. To define the depth of the mantle that corresponds to such events, this study also specified the upper and lower band of the gravity signal range between the spherical harmonic degree of 13 and 25.

1.3 Objectives of the Study

1.3.1 General Objective

The goal of this study is to determine the horizontal stress and assess its temporal variation at the base of the lithosphere due to the mantle convection in East Africa Great Rift Valley via a gravimetric approach.

1.3.2 Specific Objective

The following specific tasks are conducted through the study to succeed in meeting the general objective of this thesis

- Evaluate the lithospheric shear stress using the static gravity field
- Evaluate and compare the lithospheric shear stress using different static gravity field models
- Asses the temporal variations of lithospheric shear stress using the GRACE monthly data solution

1.4 Research Question

Once having an answer to these main questions stated below, enables the study to achieve the solution of a problem in this thesis.

- How much effective is the gravimetric approach to show the lithospheric shear stress and its temporal variation due to mantle convection?
- How does various geophysical information are going to incorporate into the gravimetric approach?
- Where does major lithospheric horizontal stress is significant? And does it have a reasonable correlation with Seismic activities and the existing World Stress Map?

1.5 Significance of the Study

Different geoscience disciplines utilize up-to-date and reliable gravimetric data to acquire knowledge about various phenomena of earth systems associated with climate systems, solid earth geophysical, and so on, for instance, by using static gravity data, GRACE/GRACE-FO data and

GOCE data. This study is significant in the way that provides vital information about the state of horizontal stress and its temporal variation using a static gravity field and GRACE data over a wide geographic area, that incorporates the East African Great Rift Valley, which is the major and most active continental rift system in the world.

The study makes a contribution to the field of earth system science by using a gravimetric approach to model, analyze, and evaluate how stress events relate to various geophysical processes. It advances our understanding of the primary cause of lithosphere stress, which is mantle flow and its effects on the Earth's system. It offers a more in-depth understanding of the stress caused by the effects of mantle plumes operating at (or close to) the lithosphere's base. Such details highlight the extent of the lithospheric stress the EARS has experienced and one may see how much the lithospheric stress the EARS has endured by having this knowledge. The study is also relevant in regions without sufficient coverage by continuous global positioning system (GPS) sites. Moreover, this study gives insight and provides an impetus for further ongoing research regarding this area of interest.

1.6 Organization of the Thesis

Six chapters make up the overall structure of this thesis research, which is followed by a bibliography. Each chapter detailed the idea's chronological development rationally.

The background of the study, the statement of the problem, the objective of the study, the research questions, the significance of the study and this section as a subject, and a review of earlier studies conducted globally that were concerned with the determination of lithospheric stress are all included in Chapter 1's introductory section. The information in chapter two regarding stress, isostasy, the fundamentals of satellite gravity missions, and several methods of stress estimation is presented adequately. Three crucial characteristics are discussed in chapter three: The research area is described in the first section, data types and materials that are frequently used as input parameters are described in the second section, and the main portion of the chapter that discusses the specific techniques are presented in the third section. The study's findings are presented in the fourth chapter as a text and graphic. In general, this chapter demonstrates the lithospheric shear stress concerning the target area both in eastward and northward directions as well as its magnitude using static gravity field EGM08, the comparison of static gravity field models, and temporal variation of stress in the study area. Chapter Five deals with the discussion and interpretation of the study. Finally, chapter six concludes what has been done and recommends certain remaining works to be included in future research in the related area.

CHAPTER TWO

2. Review of Literature

2.1 Stress's Basic Theory

Stress is stated as a force exerted on the body mass by a movement of tectonic plates towards each other (Sjöberg & Bagherbandi, 2017). Tectonic stress is defined as the amount of force per unit area that acts on a mass as the Earth's lithosphere moves. The force, or stress, across a plate, depends on the direction of motion of the plate. In terms of continuum mechanics, the stress acting on a homogeneous, isotropic at depth is describable as a second-rank tensor with nine components as

$$\bar{S} = \begin{pmatrix} S_{11} & S_{12} & S_{13} \\ S_{21} & S_{22} & S_{23} \\ S_{31} & S_{32} & S_{33} \end{pmatrix} \tag{2}$$

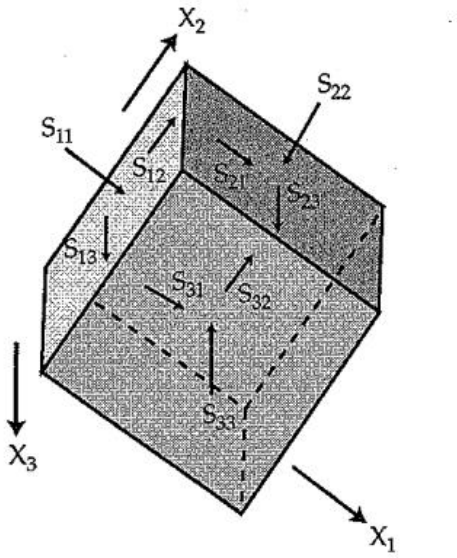

Figure 1 Description of stresses in 3-D (M. D. Zoback & Zoback, 2002)

The subscripts of each stress component indicate the direction in which a particular force is operating the face of the unit cube upon which the stress component acts. Thus, in simplest terms, any given stress component represents a force acting in a specific direction in a unit area of a given orientation. As shown in figure 1 a stress tensor can be defined in terms of any arbitrary reference frame.

$$S_{12} = S_{21}$$
$$S_{13} = S_{31} \quad (2.1)$$
$$S_{23} = S_{32}$$

Due to the equilibrium requirement, the subscripts' order is not significant in this situation. In general, six stress magnitudes or three stress magnitudes and three angles that determine the orientation of the stress coordinate system must be estimated to completely represent the state of stress at depth. (M. D. Zoback & Zoback, 2002) it is possible to evaluate the stress in any coordinate system via tensor transformation by determining a stress tensor. Specifying the direction cosines that describe the rotation of the coordinate axis leads to performing the transformation between the old and new coordinate systems as shown in figure 2. The equation is mathematically expressed as

$$\bar{S}' = \bar{A}^T \bar{S}\ \bar{A} \quad (2.2)$$

where

$$\bar{A} = \begin{pmatrix} a_{11} & a_{12} & a_{13} \\ a_{21} & a_{22} & a_{23} \\ a_{31} & a_{32} & a_{33} \end{pmatrix} \quad (2.3)$$

$$S' = A^T S\ A$$

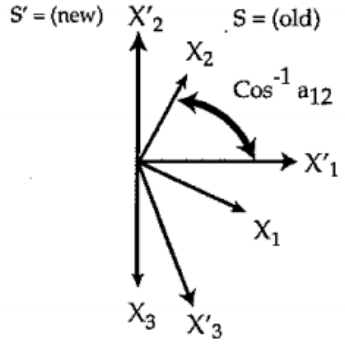

Figure 2 The tensor transformation (rotation of axis) (M. D. Zoback & Zoback, 2002)

The ability to transform the coordinate system is of interest here because we can choose generally to describe the state of stress in terms of the principal coordinate system. The principal coordinate system is the one in which shear stresses vanish and only three principal stresses, $S_1 \geq S_2 \geq S_3$, fully describe the stress field as shown in figure 3. As a result, the primary stresses and the direction of the principal stresses are reflected in the diagonalized stress tensor's eigenvectors.

$$\bar{S}' = \begin{pmatrix} S_1 & 0 & 0 \\ 0 & S_2 & 0 \\ 0 & 0 & S_3 \end{pmatrix} \tag{2.4}$$

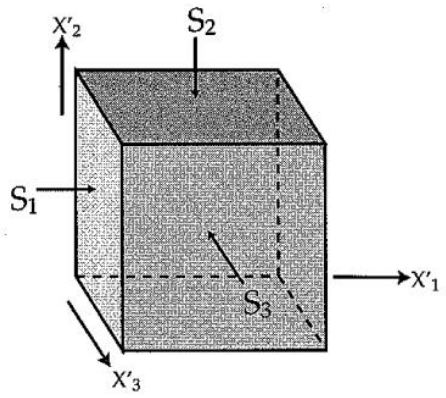

Figure 3 The Principal Stresses as defined in a coordinate system in which shear stresses vanish (M. D. Zoback & Zoback, 2002)

2.1.1 Types of Stress

There are different types of stress depending on whether the force acts equally in all directions or with different magnitudes in different directions, the force acting on a surface could be uniform or differential respectively. Compression, tension, and shear stress are the three basic types of stress in geoscience (Sjöberg & Bagherbandi, 2017). Compression is the type of stress that is firmly pressed from opposite sides or all sides and a body of rock becomes denser. Mostly the amount of space taken by that rock diminishes and pushes either higher up or deeper down into the crust. It happens at convergent plate boundaries and forms a mountain. When an area of land is forced over the top of another area of land at a low angle trust fault appears. Tension is stress that extends across and pulls a body of rock separately to or on one side. When it happens, the rocks tend to become thinner. It takes place at or near divergent plate boundaries and happens in a continent and oceanic crust and they can form continental and ocean ridges respectively. The fault made by this type of stress in nonoceanic regions is called a normal fault. Shear stress is the stress component parallel to a given surface. It results from forces exerted parallel to the surface or forces transmitted through the surrounding rock that are exerted far away. It occurred at transform boundaries and the lithosphere neither is created nor destroyed. In this case, no major topographic effect or volcanic activity appears. It results in a strike-slip fault when two objects are sliding over each other.

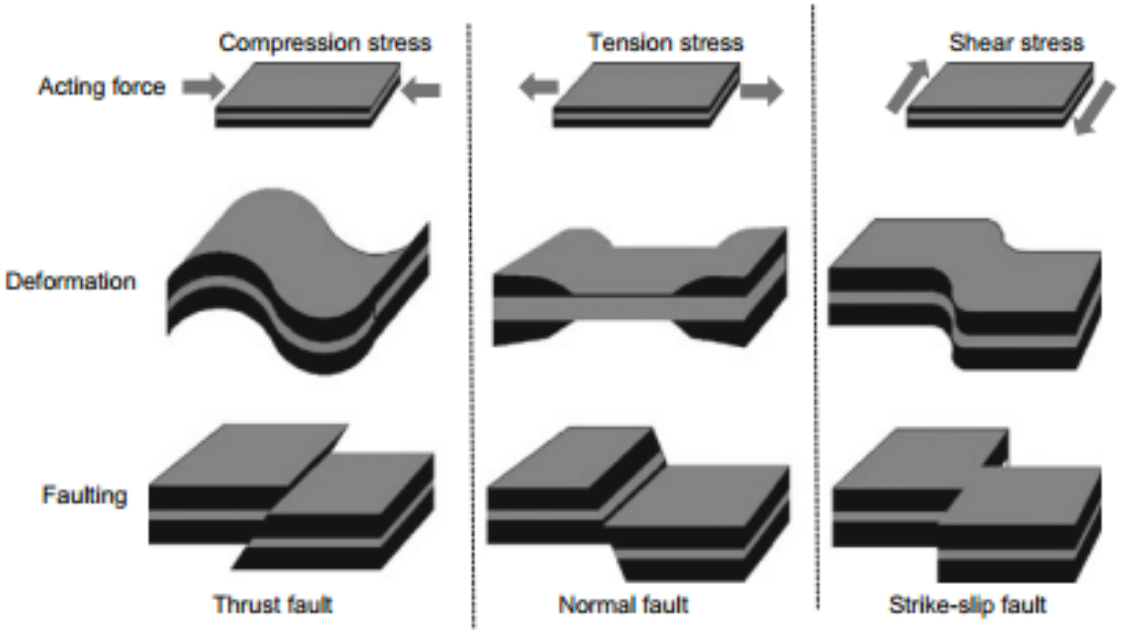

Figure 4 Different types of stress acting on a surface (Sjöberg & Bagherbandi, 2017)

2.2 Satellite Gravity Mission

The gravity field reflects the mass inhomogeneities in the earth's interior and on the earth's surface. Also, it is fundamental for the determination of the geoid which, in turn, may be regarded as a physical reference surface for various geodynamical processes and their interaction. However, at long-term time scales, the time-variable gravity field is affected by different earth's geophysical and geodynamical processes. In earth system research, this observable gravitational change offers a special tool for investigating and tracking mass transfer. This implies the accuracy requirement in geoscience for detailed gravity field information amount to 1mgal for gravity anomalies and the related accuracy for the geoid ranges from 1cm to 2cm too.

However, the determination of temporal variations of the gravity field with adequate accuracy has been challenging. Historically, in the pre-satellite era, the earth's gravity field was known with high accuracy only in a few regions of the world. Primarily the available accurate gravity field was based on terrestrial and airborne measurements. This implied that in a large part of the world, there were virtually no gravity data available (Hofmann-wellenhof & Moritz, 2005). Currently, satellite geodesy set a new milestone, in which, that brought a completely new era of measuring temporal variations of the Earth's gravity field with unprecedented temporal and spatial accuracy, and also opened up a new avenue of opportunities for studying large-scale mass redistribution and transport in the Earth system.

Three different measurement concepts evolved, leading to three different gravity field satellite missions. The satellite-to-satellite tracking (SST) in high-low mode is realized by the "Challenging Minisatellite Payload" (CHAMP) mission, the second one is SST in low-low mode being realized by the "Gravity Recovery and Climate Experiment" (GRACE) and the third one is satellite gravity

gradiometry the objective of the “Gravity field and Steady State Ocean Circulation Explorer” (GOCE) mission (Hofmann-wellenhof & Moritz, 2005).

2.2.1 Gravity Recovery and Climate Experiment (GRACE) & GRACE-FO

The Gravity Recovery and Climate Experiment (GRACE) is a dedicated twin satellites gravity mission, jointly sponsored by NASA and DLR (German Aerospace Center) under the NASA Earth System Science Pathfinder Program launched on March 17, 2002. It provided the scientific community with very useful information concerning the time-variable nature of the Earth’s gravity field (Chen, 2018). The GRACE mission allows for the first time for the recovery of the global gravity field down to spatial scales of a few hundred kilometers with a temporal resolution of monthly and even sub-monthly intervals. Due to the GRACE gravity data's ability to quantify current mass redistributions associated with these phenomena at the earth's surface, such unheard-of data is crucial for a thorough understanding and modeling of geophysically driven processes. (Schmidt et al., 2008).

In more than 15 years long record of GRACE time-variable gravity solutions radically changed the studies of various geoscience disciplines. Additionally, GRACE made ground-breaking measurements of the ongoing worldwide shift in mass, which have greatly advanced our knowledge of the large-scale alterations in polar ice, soil moisture, surface and ground water storage, and ocean mass distribution. Latterly, the Gravity Recovery and Climate Experiment Follow-on (GRACE-FO) mission launched on May 21, 2018, succeeds the GRACE mission, with a similar satellite orbit configuration and improved system design. The GRACE-FO’s primary mission goal is to continue the tracking of Earth's mass movements and changes, in particular those related to water. A collaboration between NASA and the German Research Centre for Geosciences (GFZ) has resulted in the GRACE-FO project. (Cooley & Landerer, 2020). However, a temporal gap exists from July 2017 to May 2018 between the GRACE and GRACE-FO missions, which is not ideal but would not affect most related applications focusing on seasonal and long-term time scales (Boergens et al., 2020; Landerer et al., 2020).

Monthly GRACE global gravity solutions are provided by three GRACE data processing centers forming the Science Data System (SDS), including the Center for Space Research (CSR) at the University of Texas at Austin, German Research Centre for Geosciences (GFZ), and the NASA Jet Propulsion Laboratory (JPL). The provided time series consists of monthly and long-term mean sets of spherical harmonic coefficients of the global gravity potential of the Earth. These are easily translatable into any surface mass anomalies or gravity functional anomalies in the space domain as needed for the specific application. Since the mission's debut, the SDS teams have issued the number of releases, and the quality of these models has greatly increased from release to release thanks to several thorough revisions and reprocessing of the GRACE data sets, which are continually growing (Schmidt et al., 2008).

2.2.2 Instrument Design

The so-called satellite-to-satellite tracking idea in the low-low mode (low-low SST) has been realized for the first time with the GRACE mission. The instruments on GRACE and GRACE-FO (noted as GRACE/GRACE-FO hereafter unless for separate discussions) were designed to enable measurements of the mean and time-variable components of the Earth’s gravity field variations.

GRACE/GRACE-FO's two satellites that follow each other, placed in low orbit configuration around the Earth, with separation by a mean inter-satellite distance of approximately 220 km, initial altitude of ~ 500 km, and an almost polar inclination of 89.5º. This configuration allows the detection of the gravity signals in the inter-satellite data well above the micron level and yields a global coverage. (Cooley & Landerer, 2020). GRACE/GRACE-FO satellite is equipped with the KBR system, a SuperSTAR Accelerometer (ACC), GPS receiver/antenna, Star Cameras, and Laser Retro Reflectors to complement the science instruments. Both satellites can maneuver into the lingering atmospheric wind in either the leading or trailing positions, forward or backward. Small changes in the distance between the two satellites, which result from the variable pull of gravity on each as they pass over the Earth's surface, make up the measurement.

The variations in the separation distance of the satellites are measured by a microwave ranging system. K-Band Ranging (KBR) System precisely measures the changes in the separation between the two GRACE satellites using phase tracking of K-band (~24 GHz radio frequency) and Ka-band (24 GHz radio frequency) microwave signals sent between the two satellites in a configuration known as DOWR (Dual One Way Ranging). The range variations can be reconstructed from these phase measurements and its numerically derived derivatives, along with other mission and ancillary data, are subsequently analyzed to compute the parameters of an Earth gravity field model that reflects the planetary mass distribution for a particular month (Bettadpur, 2003; Cooley & Landerer, 2020; Save, 2019). Also, the position of the satellite over the Earth can be determined, within a centimeter or less, by referencing the microwave ranging instrument to an ultra-stable quartz clock combined with precise Satellite GPS receivers. The non-gravitational accelerations on each satellite (i.e., air drag, solar radiation pressure, and attitude control activator operation) measured by a highly accurate electrostatic, temperature-controlled accelerometer, which is located at each satellite's center of mass, ensure that the distance measurements only considered accelerations caused by gravity. Moreover, the precise attitude references of the satellites provided by the star cameras (three on GRACE-FO, two on GRACE) mounted close to the accelerometer on each satellite (Cooley & Landerer, 2020). In addition, the GRACE-FO satellites have an experimental Laser Ranging Interferometer (LRI), which is designed for future generations of satellite gravimetry missions, to make the measurement of the separation distance between the two spacecraft (the primary measurement) even more precise.

The accuracy of KBR and ACC measurements, satellite orbits (altitude, inclination, and inter-satellite distance), data editing, and calibration (satellite measurements to gravity field) procedures, among other things, all affect the spatial resolution and accuracy of GRACE/GRACE-FO time-variable gravity solutions(Cooley & Landerer, 2020).

2.3 Isostasy

The term isostasy is derived from the Greek words "iso" and "stasis" meaning "equal standing". This term is used to explain the state of the Earth's crust and mantle behave, in the absence of disturbing force. In its simplest form, it deals that the lighter crust is floating in the dense mantle situated under. Therefore, it is an idealized state, in which, a condition of rest and quiet.

When considering the topographic masses and ocean waters as deviations from hydrostatic equilibrium, the removal of topography and the filling of the oceans should create an equilibrium

figure, with a gravity field approximately coinciding with the normal gravity field. However, from the systematic behavior of the residual gravity field quantities, it follows that the visible mass excesses and deficiencies are, to a large part, compensated by a corresponding mass distribution in the interior of the Earth (Torge & Müller, 2012). The gravity field surrounding the mountains, specifically the deflections of the plumb line, could only be explained by assuming that under every mountain range, there was also a "root" made from lighter rock species. The origin of this root was speculated to be the almost hydrostatic behavior of the Earth's crust over geological time-scales. This assumption of hydrostatic equilibrium was called the hypothesis of isostasy, also isostatic compensation (Vermeer, 2020). In isostasy, there is a line of equality at which the mass of land above the geoid is compensated by the masses below the geoid. The computational removal of both the topography and its isostatic compensation from the measured quantities of the gravity field is called isostatic reduction.

A state of isostatic equilibrium in which segments of Earth's crust float at levels determined by their thickness and density is attained by the composition and flow of material in the mantle by the following equation (Sjöberg & Bagherbandi, 2017).

$$\int_{R-D}^{R+H} \rho dh = 0 \tag{2.5}$$

where ρ is the density of the crust and D is the depth of compensation. This simple model suggests that the solid-Earth topography, with height $H > 0$ on the continents and $H < 0$ as ocean depth on the ocean.

The transport of material over the Earth's surface during the waxing and waning of ice sheets, sedimentation, and volcanism, however, disturbs isostasy and some cases that prevent equilibrium from being achieved. To explain different theories about isostatic compensation various models of isostasy, for instance, Pratt-Hayford's Isostasy Model, Airy Heiskanen's Isostasy Model, Vening Meinesz's Isostasy Model, Sünkel's Model, and Vening Meinesz-Moritz' crustal model was developed.

Pratt-Hayford's Isostasy Model is based on the main assumption that a constant isostatic compensation depth and a variable topographic density. As stated by this assumption density in and under the mountains is smaller than under the valleys or the oceans. The compensation layer situated beneath the mountain extends till to the compensation depth, in which, equilibrium prevails. However, Airy Heiskanen's Isostasy Model assumption is based on a constant topographic density with a variable compensation depth. In other words, it assumes that the solid Earth's crust floats on the viscous and denser mantle. According to this assumption, mountains have roots beneath them, meaning that the crust is thicker in mountainous areas than in oceans (Bagherbandi, 2011).

Vening Meinesz's Isostasy Model adds a regional isostatic correction based on the flat Earth assumption since the Moho density contrast is constant while the Moho depth is changeable. This concept describes the crust as a uniform elastic plate resting atop a viscous mantle. As a consequence, the local compensating masses of the mountains are distributed laterally and reduced

from the center of the region towards the margin. Moreover, this model states that until the isostatic equilibrium condition attains the load of the topographic mass causes the Earth's crust to bend (Sjöberg & Bagherbandi, 2017). In Sünkel's Model, the Earth's crustal thickness is estimated by introducing a smoothing factor in Airy-Heiskanen's model and adopting a regional compensation. Also, to estimate the depth of isostatic compensation, this model deals with the global topographic models and defines some criteria i.e., the norm of the residual potential of topographic and compensating masses, should be a minimum (Sjöberg & Bagherbandi, 2017).

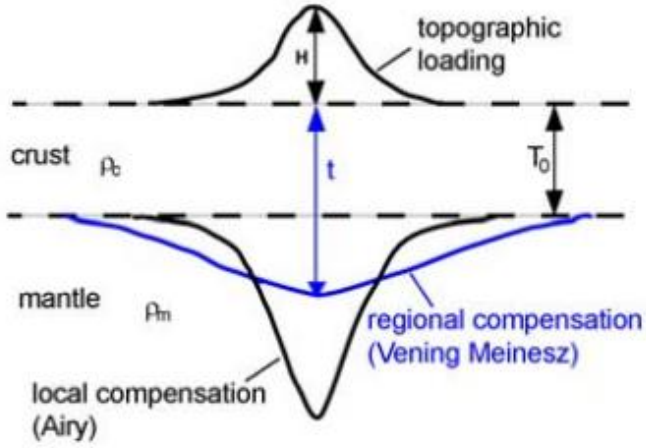

Figure 5 Comparison of the local and regional compensation of the topographic masses (Sjöberg & Bagherbandi, 2017)

2.3.1 Vening Meinesz-Moritz' Crustal Model

(Moritz, 1990) generalized Vening Meinesz's theory from a regional isostatic compensation to global compensation, and replaced the flat Earth approximation model with a spherical earth model (i.e., the reference ellipsoid is approximated by a sphere and normal gravity is from a homogeneous sphere of the same mass as the Earth). (Sjöberg, 2009) further developed it mathematically and expressed as Vening Meinesz–Moritz (VMM) isostasy. In this model, gravimetric data is introduced for expressing the isostatic equilibrium (Sjöberg, 2013).

The Vening Meinesz-Moritz problem (Moritz, 1990; Vening-Meinesz, 1931) is to determine the Moho depth D such that the compensating attraction A_C compensates the Bouguer gravity anomaly Δg^B on the Earth's surface, implying that the isostatic gravity anomaly Δg^I vanishes for point P on the Earth's surface (Sjöberg, 2009).

$$\Delta g^I = \Delta g^B + A_C = 0 \tag{2.6}$$

Whereas Δg^B and A_C are the refined Bouguer gravity anomaly and compensation attraction respectively. Equation (i) is not exact in practice, as there may be local deviations from isostatic equilibrium, even if it is theoretically accurate. The isostatic inverse problem according to VMM's hypothesis is based on a constant density contrast $\Delta\rho = \Delta\rho_m - \Delta\rho_c = \text{const}$, and a variable Moho

depth (Moritz, 1990). (Sjöberg, 2009) divided the compensation attraction into two terms. In this decomposition the compensation attraction A_C is

$$A_C = A_{C_0} + dA_C \tag{2.7}$$

where the first A_{C_0} and the second terms dA_C are the mean and residual compensation attractions, respectively.

By inserting Eq. (2.7) into Eq. (2.6), the residual compensation attraction is obtained:

$$dA_C = -\Delta g^B - A_{C_0} \tag{2.8}$$

Equations (i) and (iii) are the main equations of the inverse problem of the VMM, and the Moho depth can be determined by the Bouguer gravity anomaly and the compensation attraction. We can obtain the normal compensation attraction A_{C_0} and the residual compensation attraction dA_C (Sjöberg, 2009):

$$A_{C_0} = \frac{4\pi kR}{3}\left[\left(1-\tau_0\right)^3 - 1\right] \approx -4\pi kD_0 \approx -4\pi G\Delta\rho D_0 \tag{2.9}$$

and

$$dA_C = kR\iint_\sigma K\left(\psi,\tau\right)d\sigma \approx 2\pi G\Delta\rho D \tag{2.10}$$

Here $k = G\Delta\rho$, $\tau_0 = \frac{D_0}{R}$, and $\tau = \frac{D}{R}$ where G is the Newtonian gravitational constant, σ is the unit sphere, D_0 is the mean Moho depth, D is the (actual) Moho depth. Hence, if there is a discrepancy between the real and the mean Moho depths, then an apparent density anomaly $\Delta\rho$ arises within a depth range between D_0 and D (Moritz, 1990).

The integral kernel *K* in Equation (2.10) is a function of parameters ψ and $s = 1-\tau$; where ψ is the geocentric angle between the computation and integration points. The spectral of *K* (Sjöberg, 2009)

$$K\left(\psi,s\right) = \sum_{n=0}^{\infty}\frac{n+1}{n+3}\left(1-s^{n+3}\right)P_n\left(\cos\psi\right) \tag{2.11}$$

Where P_n is Legendre polynomials.

2.4 Techniques to Determine Stress

2.4.1 Determining Stress Using Geometric Geodesy Technique

The pattern of present-day relative plate tectonic motions in terms of direction, as well as the amount of displacement, were performed by a traditional trilateration method of survey i.e., electronic distance measurement and angle observations using theodolites. However, more

recently Global Navigation Satellite Systems (GNSS), Very Long Baseline Interferometry (VLBI), Satellite Laser Ranging (SLR), Interferometric Synthetic Aperture Radar (InSAR), and Differential Radar Interferometry data are commonly used (Sjöberg & Bagherbandi, 2017).

Global Navigation Satellite Systems (GNSS)

Global Navigation Satellite System (GNSS) has drawn the attention of scientists and users all over the world for its wide-ranging Earth observations and applications. GNSS is comprised of fully global operational satellite navigation systems, such as BeiDou Navigation Satellite System (BDS), Galileo, GLONASS, and GPS, which have been widely used in earth science studies. The recent development of GNSS networks enables to study of ongoing crustal deformation within a spatial and temporal resolution extent. GNSS geodetic measurements have been employed widely to investigate Tectonic plate motion and seismic deformation, Landslide and geological movements, Earth rotation, Tidal motion, Mass transport, and deformation (Sjöberg & Bagherbandi, 2017). For example, GNSS observation i.e., GPS data observed in a permanent station was used in assessing the stress due to the GIA is likely combined with the other sources of the stress i.e., the stress triggered by the mantle convection in Fennoscandia. the result shows that the horizontal motion diverges from the center of the land uplift dome and there is a geometrical similarity with the stress determined by Runcorn's method (Gido et al., 2018).

Very Long Baseline Interferometry (VLBI)

This technique originated from the field of radio astronomy which is independent of the gravity field. The basic observational part of a VLBI configuration consists of two radio telescopes, two atomic clocks, and two recording units. These equipment are used to measure the primary geodetic observable i.e., the time delay.

The telescopes on the earth received a radio signal from the astronomical radio source together with the timing signals from an ultra-stable oscillator and then delivered to the VLBI data processing facility and played back through the correlator, in which, the associated time delay (i.e., the difference in signal arrival time at the two antennas) is calculated to determine the bassline between the radio telescopes. This enables to improvement the angular sensitivity and resolution of a radio telescope with a size equal to the maximum separation between the telescopes. The quantity of time delay is the most important VLBI observable for geodetic applications such as very precise distance measurements on the Earth's surface and assists us in our understanding of its interior, atmosphere, and oceans, estimating Earth's rotation rate, determining Earth's orientation in space, a realization of a stable reference frame and so on. Nowadays, establishing fixed-station of geodetic VLBI network for a regular basis of observation and attaining a baseline measurement between geodetic VLBI stations with an accuracy of better than 2 mm, provides a way to determine surface deformation as well as strain rate (Seeber, 2003; Sjöberg & Bagherbandi, 2017).

Satellite Laser Ranging (SLR)

The SLR configuration system consists of a laser and transmitting and receiving telescopes. SLR technique observes the time of flight of a laser pulse as it travels between a ground station and a

satellite. At the ground station, a short laser pulse is generated and transmitted through an optical system to the satellite equipped with retroreflectors, which reflect the outgoing pulse. While the incoming reflected pulse is received, detected, amplified, and analyzed on the ground station. Then the round-trip time is measured, and scaled into the distance, with the signal propagation velocity. So far as, this precise instantaneous range of measurements at the millimeter level, leads to provide important scientific data for tectonic stress in the Earth's crust.

The ability to determine the temporal mass redistribution of the solid Earth, determine the crustal motion, measure changes in the earth's gravity field concerning the reference frame as well as capability of monitoring the vertical motion, enables the SLR system vital for the determination of plate tectonics (i.e., unique for modeling and assessing long term deformations and changes) of the earth (Seeber, 2003; Sjöberg & Bagherbandi, 2017).

Interferometric Synthetic Aperture Radar (InSAR)

InSAR is a radar technique that uses two or more Synthetic Aperture Radar (SAR) images to generate maps of surface deformation (topography) or Digital Elevation Models (DEM), using differences in the phase of the waves returning to the satellite or aircraft. In this technique, at a slightly different antenna position, a second image of the same ground scene is recorded either simultaneously with the single-pass interferometer or during a different pass by the same or another satellite after several days or even months with repeat pass interferometry. This technique within a range of days to years can potentially measure millimeter-scale changes in deformation, which enables to study of surface displacements related to tectonic deformation (Seeber, 2003; Sjöberg & Bagherbandi, 2017).

Differential Radar Interferometry

Differential Radar Interferometry or Differential Interferometric Synthetic Aperture Radar (D-InSAR) technique is employed, when three or more SAR images of the same area, are generated from different passes at approximately the same antenna position. It is possible to have at least two interferograms, that can be differenced and creates a differential interferogram. When surface changes occurred between the times of observation and also caused a change in the slant range to the antenna, phase changes were exhibited in the differential interferogram.

Hence it reveals surface changes like swelling and buckling with a resolution of centimeters or even millimeters, this technique is capable to provide a highly detailed and accurate picture of crustal deformation by combining effectively with other geodetic techniques like GNSS (i.e., continuous GPS arrays) (Seeber, 2003).

2.4.2 Determining Stress by Disturbing Potential Components

Long-to-medium wavelengths of the Earth's gravity field can be utilized to study large mass distributions and irregularities in the Earth's layers. (Runcorn, 1967) estimated the stress between two different Earth layers using the Navier-Stokes equation. He assumed that the upper part of the Earth consists of two layers (the outer layer being the rigid crust and the inner viscous layer being the mantle), which satisfy the following conditions:

1) The size of the upper part of the Earth is large enough so that the gravitational effect of the lower boundary can be neglected, and
2) the shape of the upper boundary is such that it is hydrostatic equilibrium.
3) it assumes that the mantle viscosity coefficient is constant.

Under these conditions and assuming that the disturbing potential of the Earth's gravity field (T) (Runcorn, 1967) gives the stress components exerted by the mantle convection on the crust in the east-west and north-south directions as follow:

$$\sigma_X = \frac{MG}{4\pi R^2}\sum_{n=2}^{n_{\max}}\left(\frac{R}{R-D_0}\right)^{n+3}\frac{2n+1}{n+1}\sum_{m=-n}^{n}C_{nm}Q_m(\lambda)\frac{\partial\bar{P}_{n|m|}(\theta)}{\partial\theta} \tag{2.12}$$

$$\sigma_Y = \frac{MG}{4\pi R^2}\sum_{n=2}^{n_{\max}}\left(\frac{R}{R-D_0}\right)^{n+3}\frac{2n+1}{n+1}\sum_{m=-n}^{n}mC_{nm}Q_{-m}(\lambda)\frac{\partial\bar{P}_{n|m|}(\theta)}{\sin\theta} \tag{2.13}$$

M is the mass of the Earth, G is the gravitational constant, R is Earth's mean radius, D_0 is the mean Moho depth, θ is co-latitude, λ is longitude.

and

$$\frac{\partial\bar{P}_{n|m|}}{\partial\theta} = \frac{1}{2}\left[(n+|m|)(n-|m|+1)P_{n,|m|-1} - P_{n,|m|+1}\right] \tag{2.14}$$

Finally, the magnitude (S) of the stress can be expressed by:

$$S = \sqrt{\sigma_X{}^2 + \sigma_Y{}^2} \tag{2.15}$$

2.4.3 Determining Stress Using a Gravimetric-Isostatic Crustal Model

This method is going to discuss an alternative method to study horizontal stress using the gravity disturbance determined from the gravimetric-isostatic crustal model. This method uses a known Moho depth model, obtained from CRUST1.0, for predicting δg (The free-air gravity disturbance) and then the Earth's gravitational potential (T). The obtained disturbing potential will be used to determine the sub-lithosphere horizontal stress due to the geodynamical movement e.g., mantle convection.

Using traditional isostatic gravity disturbance according to the Vening Meinesz-Moritz (VMM) model (Sjöberg, 2009, 2013) as follow

$$\delta_g^I = \delta_g^B + A_C = \delta_g - A^T + A_C \tag{2.16}$$

Where: - δ_g^B is the Bouguer gravity disturbance and A^T is the direct effect on gravity.

The traditional Bouguer gravity disturbance using A^T will be no-topography gravity data given by (Sjöberg et al., 2015)

$$\delta_g^B = \delta_g - A^T \tag{2.17}$$

The topographic gravity disturbance effect is computed as follows

$$\delta_g^T = -A^T = \frac{\partial V^t}{\partial r_P} \tag{2.18}$$

Where: - δ_g^T is the topographic gravity disturbance, V^t is the topographic potential, and r_P is the geocentric radius of any point *P* with angular spherical coordinates (spherical colatitude and longitude).

Using the gravitational potential harmonic that can be expanded into an external harmonic series for the computation point to be outside the topographic masses Then the attraction of the topographic masses, A^T become

$$A^T(P) = \sum_{n=0}^{\infty} \frac{n+1}{R} \sum_{m=-n}^{n} \left(\frac{R}{r_P}\right)^{n+2} V_n^t(P) \tag{2.19}$$

Where: - V_n^t is the spectral contribution of degree n to the topographic potential V^t.

The free-air gravity (δg) can be determined by the condition that isostatic gravity anomaly δ_g^I vanishes

$$\delta_g^I = 0 \tag{2.20}$$

and the isostatic compensation attraction A_C is computed according to Equation (2.7).

The free-air gravity disturbance from a known Moho depth can be obtained by inserting Equations (2.9), (2.10), and (2.18) in (2.7);

$$\delta_g = A^T - \frac{4\pi G\Delta\rho R}{3}\left[\left(1-\frac{D_0}{R}\right)^3 - 1\right] - 2\pi G\Delta\rho D \tag{2.21}$$

By differentiating disturbing potential w.r.t. *r* and changing sign, we can obtain a harmonic series for the gravity disturbance in Laplace harmonics *Tn* (Ω):

$$\delta_g = -\frac{\partial T}{\partial r} = \sum_{n=0}^{\infty} \frac{n+1}{R}\left(\frac{R}{r}\right)^{n+2} T_n(\Omega) \tag{2.22}$$

This yields the following relation between Laplace harmonics of the gravity disturbance and the disturbing potential:

$$\delta g_n = \frac{n+1}{R} T_n \tag{2.23}$$

and

$$T_n = \frac{R}{n+1}\delta g_n \tag{2.24}$$

Inserting Equation (2.22) in (2.25) and summing up the terms the disturbing potential will be obtained as:

$$T = \sum_{n=0}^{n_{\max}} \sum_{m=-n}^{n} \frac{R}{n+1}\left(A^T - \frac{4\pi G\Delta\rho R}{3}\left[\left(1-\frac{D_0}{R}\right)^3 - 1\right] - 2\pi G\Delta\rho D \right) Y_{nm}(P) \tag{2.25}$$

and by using harmonic analysis the coefficients C_{nm} can be obtained by

$$C_{nm} = \frac{1}{4\pi}\iint_{\sigma} T Y_{nm}(P)\, d\sigma \tag{2.26}$$

and C_{nm} will be used in Equations (2.12) and (2.13) to estimate the sub-lithosphere stress components due to the geodynamical movements triggered by mantle convection.

2.4.4 Determining Stress Using GRACE

The GRACE sensors are appropriate tools to measure secular gravity changes in the Earth's different layers. There are different solutions and data sorts for GRACE monthly, weekly, and 10-days solutions provided by several analysis centers.

Due to the mass movement and interchange of materials across the parts of the Earth system, the geopotential at a fixed-point change throughout time. Long-term monitoring of temporal stress change using GRACE data is important for updating the absolute stress model which is the most significant responsible phenomenon for the gravity change (and sub-lithosphere stress change).

Assuming linear regression in time (t_i) with observation equations obtained from the GRACE mission observed at different epochs:

$$a + bt_i = l_i - \varepsilon_i \tag{2.27}$$

where the secular trend (b) of the disturbing potential (l_i). The secular trend (b) is determined using the least squares adjustment method. ε_i is the observation's random errors. In particular, if the time interval (Δt) between successive epochs is constant, it follows that:

$$\hat{b} = \frac{2}{\Delta t}\frac{\sum_{i=1}^{n}(2i-n-1)l_i}{\sum_{i=1}^{n}(2i-n-1)^2} \text{ and } s_b = \frac{2}{\Delta t\sqrt{\sum_{i=1}^{n}(2i-n-1)^2}} \tag{2.28}$$

where s_b is the standard error of $\hat{b}$, and s^2 is the variance of unit weight.

The secular trend of the disturbing potential (that is *b*) can be also written:

$$\dot{T} = \frac{GM}{R}\sum_{n=0}^{\infty}\left(\frac{R}{r_p}\right)^{n+1}\sum_{m=-n}^{n}\dot{C}_{nm}Y_{nm}(P) \tag{2.29}$$

where dot means the derivative w.r.t. time and $\dot{C}_{nm}$ can therefore be estimated by

$$\dot{C}_{nm} = \frac{1}{4\pi}\iint_{\sigma}\hat{b}Y_{nm}(P)\,d\sigma \tag{2.30}$$

Furthermore, from Equations (6) and (7) the temporal changes of the sub-lithosphere stress components become:

$$\dot{\sigma}_X = \frac{MG}{4\pi R^2}\sum_{n=2}^{\infty}\left(\frac{R}{R-D_0}\right)^{n+3}\frac{2n+1}{n+1}\sum_{m=-n}^{n}\dot{C}_{nm}Q_m(\lambda)\frac{\partial\bar{P}_{n|m|}(\theta)}{\partial\theta} \tag{2.31}$$

and

$$\dot{\sigma}_Y = \frac{MG}{4\pi R^2}\sum_{n=2}^{\infty}\left(\frac{R}{R-D_0}\right)^{n+3}\frac{2n+1}{n+1}\sum_{m=-n}^{n}m\dot{C}_{nm}Q_{-m}(\lambda)\frac{\partial\bar{P}_{n|m|}(\theta)}{\sin\theta} \tag{2.32}$$

Similarly, the change of magnitude ($\dot{S}$) is obtained by

$$\dot{S} = \sqrt{\dot{\sigma}_X{}^2 + \dot{\sigma}_Y{}^2} \tag{2.33}$$

Here it is important to emphasize that according to (Runcorn, 1967) the stress balances gravity refers to an equilibrium state and the time derivative can be used to derive stress change as a function of gravity rates. In addition, there are no “constants” that should change and make a significant problem in considering temporal changes of stress.

CHAPTER THREE

3. Materials and Methods

3.1 Description of the Study Area

The study area is geographically located between -25ºS - 30°N and 20º - 60°E. The Great Rift Valley of East Africa the so-called "Great Rift Valley System" runs from the Middle East in the north to Mozambique in the south and is arguably the most well-known rift valley on the planet. It is one of the very few significant active continental rift valleys on continental lithospheres, along with the Rio Grande Rift and the West Antarctic Rift Valley. There are volcanoes, hot springs, geysers, and regular earthquakes in this geologically active region.

The East African Rift System forms a narrow (50–150 km wide), elongate system of normal faults that stretches about 3,500 km in a sub-meridian direction and is connected to the world-wide system of oceanic rifts via the Afar Triangle to the Gulf of Aden and the Red Sea. The EARS is composed of two main rift trends, the eastern (including the Ethiopian Rift) and western branches (appears to have been initiated later than the eastern branch, during the late Miocene) of the EARS. In addition, the southeastern branch of the Mozambique Channel is the third rift trend. The eastern branch extends across a 2200 km stretch, starting at the Afar triangle in the north, passing through the major Ethiopian rift, the Omo-Turkana lows, and the Kenyan rifts, until coming to a stop in the basins of the north Tanzanian divergence in the south. From Lake Albert (Mobutu) in the north to Lake Malawi (Nyasa) in the south, the western branch spans a distance of 2100 km. The western branch also has several segments: the northern segment turns gradually from NNE to N-S and includes the basins of Lake Albert (Mobutu), Lake Edward (Idi Amin), and Lake Kivu; the central segment trends NW-SE and includes the basins of Lake Tanganyika (Lake Tanganyika is the second deepest and second largest in volume); and the southern segment primarily includes Lake Malawi (Nyasa) and smaller basins farther south. The Jordan Rift Valley is located in the system's northernmost region. The Golan Heights, which are close to Israel's borders with Syria and Lebanon, the Dead Sea, and the Gulf of Aqaba, a Red Sea inlet that divides the Sinai Peninsula from the Arabian Peninsula, are all located along the Jordan Rift Valley. The N-striking underwater basins west of the Davie ridge make up the southern branch. The great lakes of Eastern Africa are mostly found in the EARS, except for Lake Victoria (the second-largest freshwater lake in the world by surface area), whose waters are maintained in a relatively low area between the high mountains belonging to the eastern and western branches (Chorowicz, 2005; Morley et al., 1999).

Even though the two branches (i.e., eastern and western branches of the EARS) are seismically and volcanically active today, they have distinct geological characteristics. They show marked differences in their igneous activity (especially their volume) and morphology. Extensive volcanism and moderate seismic activity with a focal depth usually not exceeding 15 km occurs only in the eastern branch which is surrounded by a broad regional culmination. Despite having significant absolute rift subsidence, the western branch has relatively sporadic volcanism and is not encircled by a substantial regional plateau (i.e., it is characterized by sparse volcanic activity

and frequent occurrence of large earthquakes with focal depths exceeding 30 km) (Corti, 2012; Ring, 2014).

The topographic relief of EARS is characterized by broad uplifted plateaus and narrow rift valleys. Mainly it is characterized by two large lithospheric domes, or plateaus (i.e., the Afar and East African Domes) at the largest scale, which are part of the African Super swell, a wide region of anomalously high topography that characterizes the southern and eastern portions of the African continent. The much narrower rift valley and volcanic topography of the Kenya and Western rift systems are superimposed on the approximately 1300 km wide East African dome plateau. Similarly, the narrow Ethiopian rift system and Afar depression, which lies northeast of the East African dome, and to the southwest and southeast of the Red Sea and Gulf of Aden spreading center are superimposed on the Afar dome. Turkana depression (600 m average elevation) of northern Kenya separates the Afar and East African Domes. The average elevations are 1,500 m and 1,200 m for the Afar Dome and for the East African Dome respectively. Outside of these regions, the topography varies from 300 to 900 meters. Both domes have a diameter of around 1,000 km, and significant negative gravity anomalies are linked to them. There are lesser domes (perhaps connected to magmatic underplating) within the East African Dome, including the Kivu and Kenya Domes, with radii of 100–200 km. The 500-km-wide Darfur dome is made up of the EARS in addition to the two large plateaus (Ebinger et al., 1989; Morley et al., 1999).

(Corti, 2012) The Somali and Nubian plates are created when the East African Rift Valley divides the African plate into two unequal pieces. Most of Africa is made up of the Nubian Plate, whereas the smaller plate that is separating is known as the Somalian Plate. Both of these plates are migrating away from the Arabian plate to the north as well as from one another. It is known as a triple junction where these three plates collide in Ethiopia's Afar region. The Somali plate, the Nubian plate, and the Arabian plate are all separating from one another at the Afar Triple Junction.

Divergent motions are in charge of the morphotectonics of the EARS, which causes localized extensional strain in the continental lithosphere. While the lithospheric mantle is susceptible to strongly defined ductile thinning, causing ascent of the asthenosphere mantle, the brittle crust has responded by faulting and subsidence, generating elongated narrow rifts. The narrow, elongated zones of thinned lithosphere associated with deep asthenosphere intrusions in the upper mantle, which impact the stress level in the EARS, are the most distinctive characteristics of the rift system(Chorowicz, 2005). The region underneath the southern portion of Lake Tanganyika is the focus of an extensive elongated upwelling flow system linked to tensional stress under the EARS region. The mid-Indian Ocean ridge is connected to the upwelling flow to the south and continues northward to the Gulf of Aden(Liu, 1977). Normal faults are the primary tectonic characteristics on the surface, although strike-slip, oblique-slip, and even reversal faults exist.

The Red Sea and the East African Rift Valley are recognized as major tensional tectonic features of the earth’s crust. The seismicity of the Red Sea, Gulf of Aden, and the East African Rift shows that the Nubian, Arabian, and Somalian plates meet at the south end of the Red Sea (i.e., at the Afar Triple Junction which is hot spots on the surface of the earth), marked by volcanism, high heat flow, and uplift are surface expressions of deep-seated thermal plumes rising from the mantle (Liu, 1977). Also, the study area is mainly characterized by a crustal type of Archean, early/mid-

Proterozoic, mid/later Proterozoic, and rifts and the crustal thickness ranges from 30 to 45 km (Laske et al., 2013).

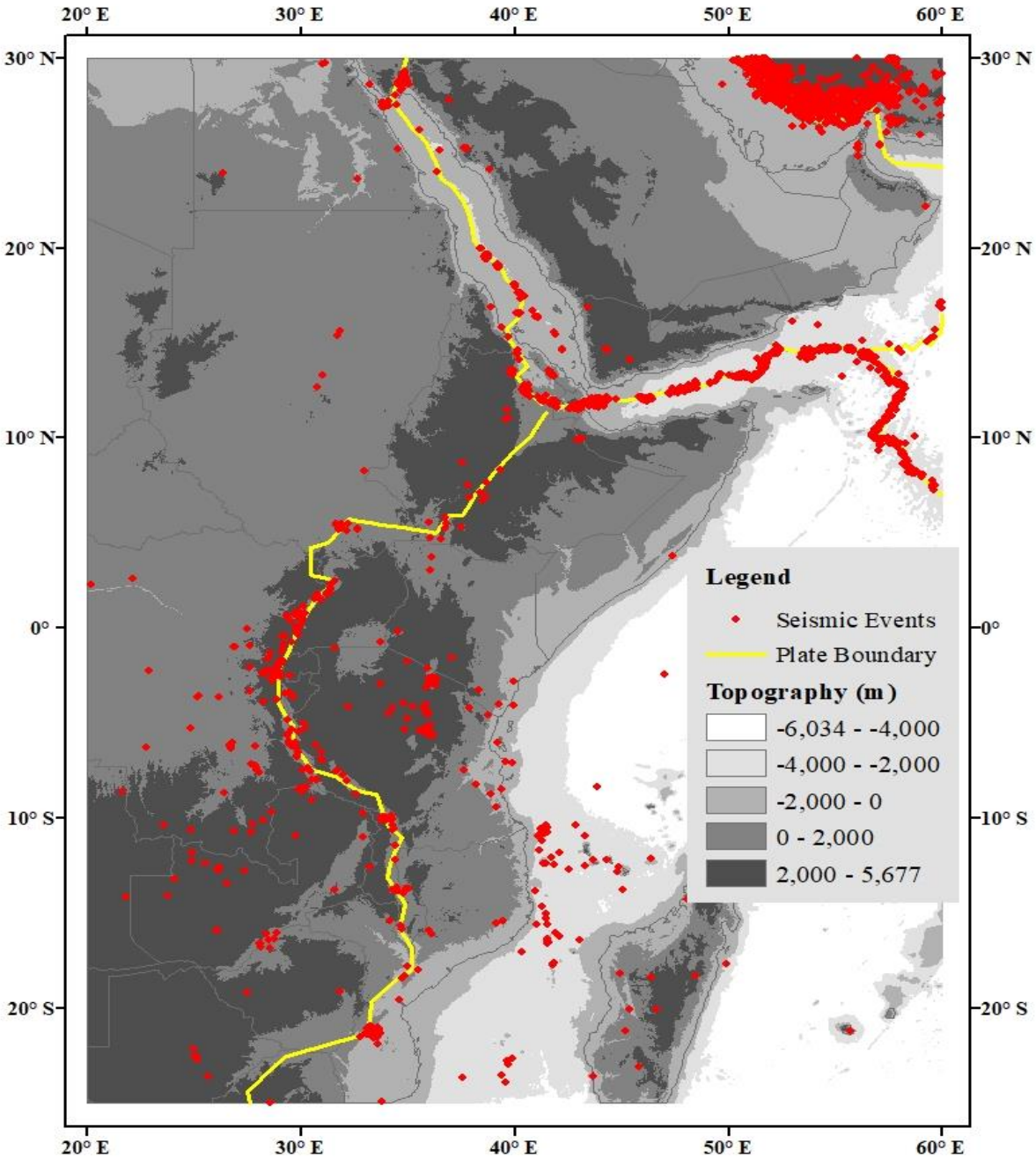

Figure 6 Location map of the study area

3.2 Data and Material Used

To achieve the objectives of this study various datasets were utilized, and also different materials were employed to process the data in carrying out this study. The description of the datasets and materials is expressed in this section. The main necessary data that are used in this study are GRACE monthly data products, lithospheric thickness, crustal thickness, and a global gravity model are the main necessary data for the computation of lithospheric stress and temporal variation result in this study area.

GRACE/GRACE-FO monthly data products are achieved from the Science Data System (SDS) center released by the Jet Propulsion Laboratory (JPL) of NASA. JPL Level-2 Gravity Field Product Release 06 and Release 06 (GFO), for GRACE and GRACE-FO monthly solutions respectively, are obtained from the ICGEM database website (http://icgem.gfz-potsdam.de/series). One of the five services overseen by the International Gravity Field Service (IGFS) of the International Association of Geodesy (IAG) is ICGEM (International Centre for Global Earth Models). The main goal of ICGEM, which is a web-based service, is to compile and archive all static temporal global gravity field models that are currently in existence and make them publicly accessible online in a standardized format with DOI numbers assigned by GFZ Data Services (i.e., offer an online interactive calculation service for the computation of gravity field functionals) (Ince et al., 2019). The monthly data products (i.e., GRACE/GRACE-FO datasets) from 2002 to 2022 existed as a maximum degree/order (d/o) of 60 X 60 and 96 X 96 individually, within a Denoising and Decorrelation Kernel (DDK) from DDK1-DDK8 and 1º X 1º resolution, in (.gfc) format. DDK is a non-isotropic decorrelation filter that uses a priori error covariance matrices derived from GRACE processing, i.e., it is based on the regularization of the normal equation. The DDK filter has several smoothing levels, with DDK1 being the strongest and DDK8 being the lowest. When the smoothing intensity is reduced, the geophysical signal is better retained, but the errors get greater and mostly appear as north-south stripes (Prevost et al., 2019). These monthly data solutions provide Earth Gravity Field models in terms of spherical harmonic coefficients used to determine the temporal variation of stress due to mantle flow, determine the rate of the gravity field change and update the absolute stress model. The GRACE/GRACE-FO data is extracted at the extent of 40 X 55 degrees according to the scope of the study area.

EGM2008 (EGM08) is developed by (Pavlis et al., 2012) through a least-squares combination of the (Institute of Theoretical Geodesy) ITG-GRACE03S gravitational model and its associated error covariance matrix. It is a 5-arc-minute equiangular grid formed by combining terrestrial, altimetry-derived, and airborne gravity data, and represents the gravitational potential of the Earth as a spherical harmonic model within the gravitational information gathered from a global set of the area mean free-air gravity anomalies. EGM2008 adds extra coefficients up to degree 2190 and order 2159 and is complete to degree and order 2159. Several products of EGM08 model development are freely available under http://earth-info.nga.mil/GandG/wgs84/gravitymod/egm2008/index.html. The ETOPO1 data is an open-source 1 Arc-Minute Global Relief Model provided by several U.S. government agencies, international agencies, and academic institutions. However, in this study, the data was obtained from the National Geophysical Data Center (NGDC), an office of the National Oceanic and Atmospheric Administration (NOAA) website

(http://www.ngdc.noaa.gov/mgg/global/global.html). The data available in "Ice Surface" (which includes the elevation at the top of the Antarctic and Greenland ice sheets) and "Bedrock" (elevation at the base of the ice sheets) versions. Both ETOPO1 versions were created using several global and regional digital data sets that were then translated to standard horizontal and vertical datums, reviewed, and adjusted as necessary. It is horizontally referred to as the World Geodetic System of 1984 (WGS 84) with a cell size of One arc-minute and vertically referenced to sea level. The data is distributed in netCDF, GRD98, binary, xyz, georeferenced tiff, pdf, png, jpeg, and kmz formats(Eakins & Division, 2009). Later, it is binned/averaged into a 1-degree cell in, CRUST1.0, a 1^{o} X 1^{o} global crustal model.

EIGEN-6C4 is a new global combined gravity field model to degree/order 2190. This model has been inferred from the combination of LAGEOS, GRACE, GOCE, and DTU ground data and contains the complete SGG data of the GOCE mission. On the continents for wavelengths beyond spherical harmonics degree 235, EIGEN-6C4 is a reconstruction of EGM2008. The data is acquired from the ICGEM database at GFZ Potsdam under the website (http://icgem.gfz-potsdam.de/tom_longtime)(Förste et al., 2014). The known Moho depth is used to calculate the thickness of the Earth's crust using the CRUST1.0 Moho model, which was created by (Laske et al., 2013) based on 1-degree averages of a newly updated database of crustal thickness data from active source seismic investigations as well as from receiver function studies. And also, the lithospheric thickness data obtained from a model developed by (Conrad & Lithgow-bertelloni, 2006) provides the lithospheric depth measured from the earth used in this study. Furthermore, the WSM2016 database (Heidbach et al., 2016) and seismic events obtained from International Seismological Center (ISC-EHB between 1964 and 2017) are also used to interpret the lithospheric shear stress and temporal variation of the stress (i.e., to validate the result by correlating with the WSM2016 and seismic events). With the addition of hydrofracturing and overcoring methods, the WSM2016 database principally consists of measured primary horizontal stress directions that are based on borehole breakout data and earthquake focal mechanisms.

The material and software that have been used in carrying out this study are MATLAB R2016b, Arc GIS 10.8, Microsoft Office, and Personal Computer. The MATLAB R2016b software package platform is used to process the data, execute all the necessary codes or equations that provide the lithospheric stress are done on it, and also to present the visual content of the results. Arc GIS 10.8 is used to process various data that lead to the display of the map of the study area. Personal Computer (Laptop) where various software used in this study are stored and also interpretations are operated is utilized. A word processor which is Microsoft Word 2019 is used for preparation of the entire document in this study. All the data and material that has been used in this study with their source summarizes in the table below.

Table 1 Summary of data and material used

No.	Data Type	Purpose	Data Source
1	GRACE/GRACE-FO	Spherical harmonic coefficients of Earth Gravity Field models	ICGEM database website
2	EGM08	To compute Earth's disturbing potential	(Pavlis et al., 2012)
3	CRUST1.0	To compute the earth's crustal thickness	(Laske et al., 2013)
4	ETOPO 1.0	To compute the topographic height	National Oceanic and Atmospheric Administration
5	EIGEN-6C4	To determine Earth's disturbing potential	ICGEM database
6	Lithospheric thickness model	To compute the lithospheric depth	Conrad and Lithgow-Bertelloni (2006)
No.	**Software and material Used**	**Purpose**	**Supplied by**
1	MATLAB R2016b	To process numerical equations	Mathworks
2	Arc GIS 10.8	To prepare maps	ESRI (Environmental Systems Research Institute)
3	Laptop	To store/install various software and accomplish each task through this study	TOSHIBA Company
4	MS Office	To prepare the entire document of the study and for statistical analyses of the result	MS Office Company

3.3 Methodology

In this section, a brief description of the general methods performed, the techniques applied, and the input datasets used in this study to carry out the horizontal shear stress at the base of the lithosphere due to flow in the mantle using a gravimetric approach based on Runcorn's theory and temporal variation of stress are presented coherently and illustrated below in Figure 7. The method enables to detection of stress and orientation throughout the study area. Moreover, to meet the objective of this study the WSM2016 and seismic events have been used for validation of the results achieved via this method.

In this method, the crustal thickness within the area of interest that refers to the mean sea level determined by using, a 1 X 1-degree global crustal model, CRUST1.0 (Laske et al., 2013) that provides a known Moho depth, as an input from which the stress is computed and for propagating to the lithosphere. The lithospheric thickness, which is measured from the earth, is computed within the extent of the study area by using the lithospheric thickness model (Conrad & Lithgow-bertelloni, 2006). The topographic height of the study area was also computed by using ETOPO1

data. Then, the depth of the base of the lithosphere, which is required to compute the sub-lithospheric stress at the base of the lithosphere, is determined by subtracting the topographic heights from the lithospheric thickness, and the result is used to estimate the lithospheric shear stress components.

After this, the spherical harmonic terms of the normal gravity field were computed by the parameters of GRS-80 for the Earth's disturbing potential based on the Earth gravitational model EGM08, that used to estimate the lithospheric shear stress components due to the geodynamical movements triggered by the mantle convection in the east-west direction and north-south direction. The low degree harmonics for $n \leq 12$ may reflect a large-scale mantle flow system (Runcorn, 1964, 1967), whereas the high degree harmonics for $n \geq 13$ may result from a short-wavelength convection system (Liu, 1977). Therefore, in this study, the EGM08 was taken over a 1^{o} X 1^{o} and synthesized to the harmonic window between degrees $13 \leq n \leq 25$ to filter the Earth's interior and a higher degree of topographic gravity signals. However, the formula lithospheric shear stress in north-south direction contains a singular term $1/\sin\theta$ in the first-order derivative of the Legendre polynomial, so this paper adopts a method to remove this singularity by using some coefficients based on (Eshagh, 2010) and it enables to synthesize the gravity gradients without computing 1^{st} and 2^{nd} order derivatives of the associated Legendre function nor singularity at the poles. Finally, once the lithospheric shear stress components are determined, the magnitude of the lithospheric shear stress can be determined.

The same wise the lithospheric shear stress is computed by using the EIGEN-6c4 static gravity field model. Then after the comparison between these different static gravity models is done by evaluating the difference of their result. The difference between the horizontal lithospheric shear stress via a static gravity field model of EGM98 and EIGEN-6C4 is computed by subtracting the result of EIGEN-6C4 from the result obtained by using the EGM98 model.

To compute the temporal variation of stress the December 2002, 2010, and 2020 GRACE/GRACE-FO monthly data solutions were used in this study. Once the data is downloaded from ICGEM database in (.gfc) format the file is converted into (.mat) format (i.e., by using *icgem2mat.m* MATLAB script code that reads geopotential coefficients from an ICGEM file and transforms them into MATLAB variables and saves them in a mat file) to process the data in MATLAB software. In this study, DDK5 filter was applied to Level-2 GRACE monthly solution to ensure a good compromise between signal retained and noise removed. Furthermore, all the processes performed to determine the static shear stress, are also applied in the same manner to compute the temporal changes of stress components in east-west and north-south directions using Runcorn's stress formula. Finally, the variation between them is computed, by taking the year 2002 as a reference and subtracting its result from the result obtained for year 2010 and 2020 of the same month distinctly.

Finally, validation of the result is performed to examine whether the results obtained in this study are in good agreement with recognized information or not. The validation is done with respect to the WSM2016 database and seismic events in the study area.

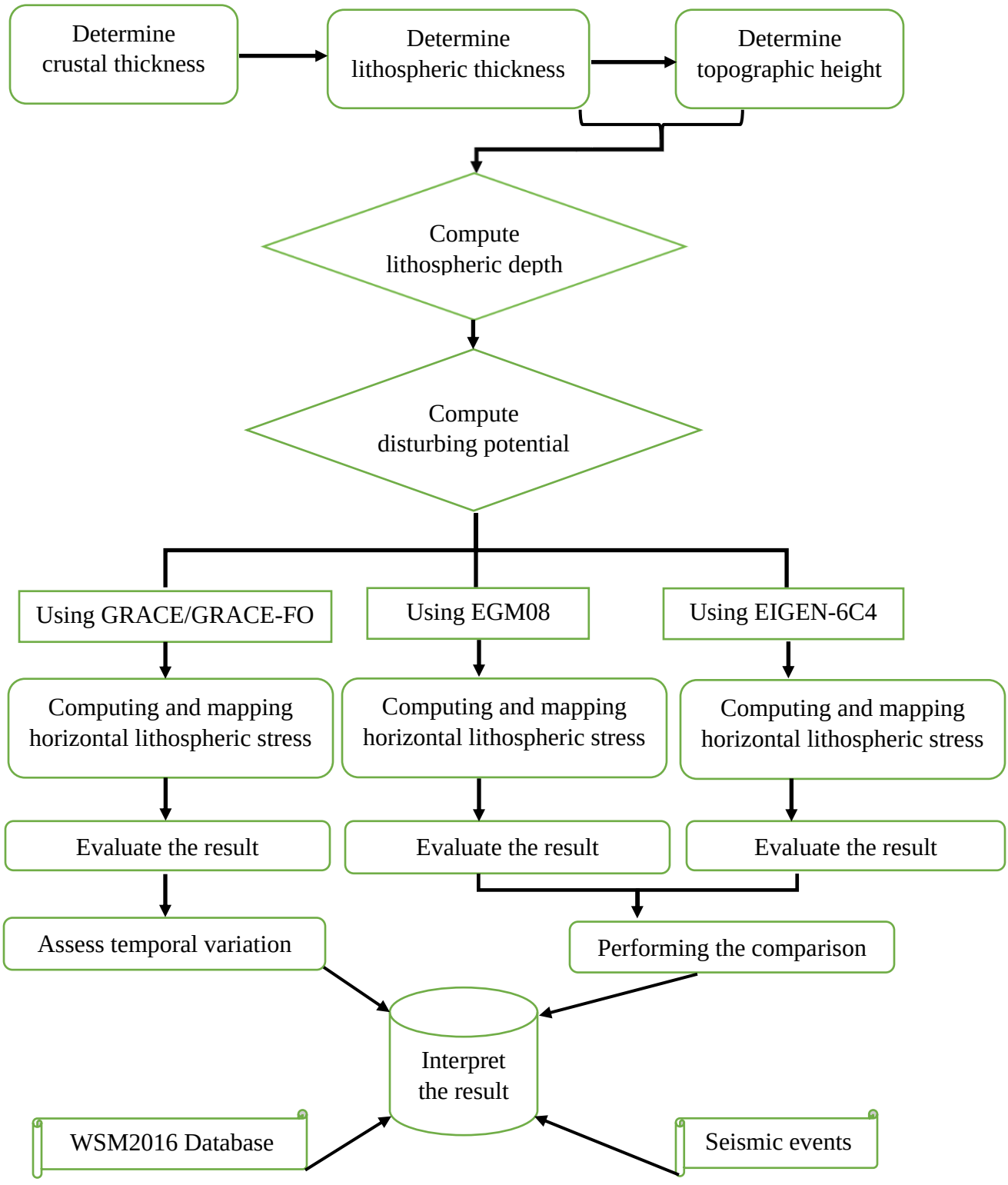

Figure 7 General Workflow of the Methodology

CHAPTER FOUR

4. Result

4.1 Lithospheric shear stress from the static gravity field

The results are obtained by carrying out all the procedures that are discussed in the method section. Figure 8 (a) and Figure 8(b) show the shear stress components under the crust of the East African Great Rift Valley exerted by mantle convection in the east-west and north-south directions respectively, that are synthesized within the spherical harmonic coefficient of degree $13 \leq n \leq 25$ range and taken over a 1^{o} X 1^{o} grid. Also, the result of the estimated lithospheric shear stress magnitude is shown in Figure 8(c). In this study, a total of 2200 pixels were used to compute the shear stress in the east-west and north-south directions. The result shows that the stresses are not only distributed near the plate boundaries (i.e., shown by the white line) but also distributed in major plates too.

The result in the east-west direction shows that the greatest extent of the magnitude of the resultant stress throughout the study area lies between, the value of -5 MPa and 5 MPa, which is 91.55% of the result obtained in the study area. The map of the shear stress component in Figure 8(a) shows the large positive value over southern Iran within the Eurasian plate (i.e., the Northeast boundary of the Asian plate), that associates with a significant strike-slip faulting and thrust faulting stress regime, in which that significant active seismicity occurred. Also, the large positive value detected in the northern part of the Red Sea (i.e., the western boundary of the Arabian plate) that associates with a normal faulting stress regime and some unknown regime where seismic activity happened. The large negative value was seen over the eastern Saudi Arabia coast, Bahrain and Qatar towards the Persian Gulf within the Arabian plate in which seismic activity was exhibited. Furthermore, the result shows the positive stress values along the plate boundaries, such that through the eastern, and western branches of the EARS, are in good agreement with the location associated with the normal faulting stress regime. In addition, some other positive values of stress were detected in the southeastern Arabian plate and continued to the western Indian plate, eastern Sudan, Tanzania, Zimbabwe, and over Madagascar. Aside from the positive stress values, negative stress values also detected in Figure 8(a) are located in western Ethiopia, the Democratic Republic of Congo, central Sudan, Egypt, eastern Libya, eastern Chad, eastern Central African Republic, western Zambia, northwest of Botswana, central Saudi Arabia that continue through the coast of east African to the coast of Mozambique and over the Indian Ocean within African plate. In this result, the positive value implies the stress orientation is in the eastward direction, whereas the negative value indicates the stress orientation is in the westward direction due to the mantle convection inside the lithosphere. Overall, 44.41% of the resultant horizontal shear stress at the base lithosphere is oriented throughout the study area in an eastward direction and the remaining 55.59% is oriented in the study area in the westward direction as depicted in Figure8(a).

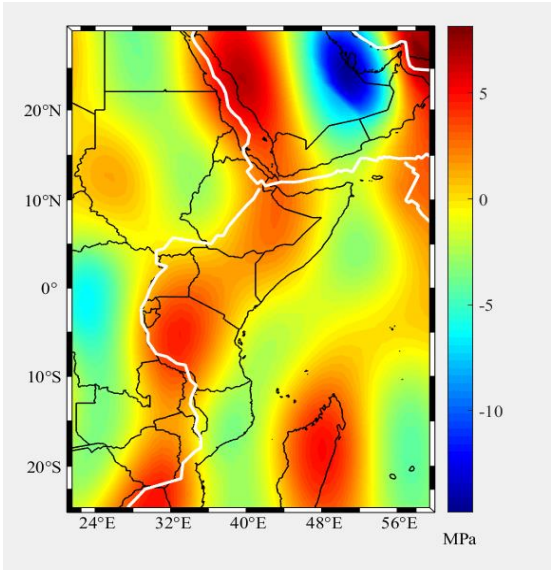

(a)

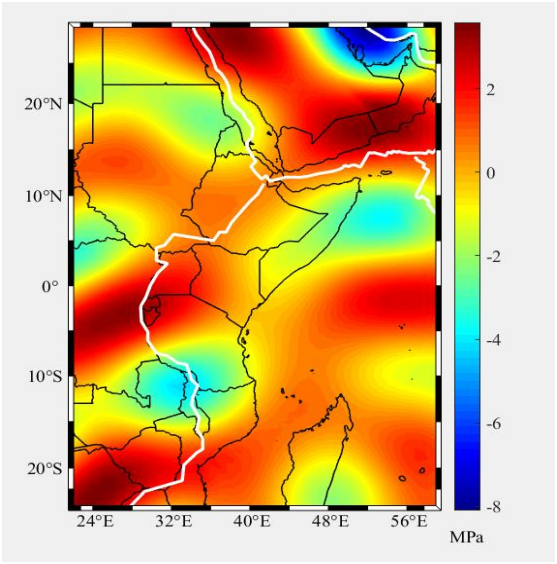

(b)

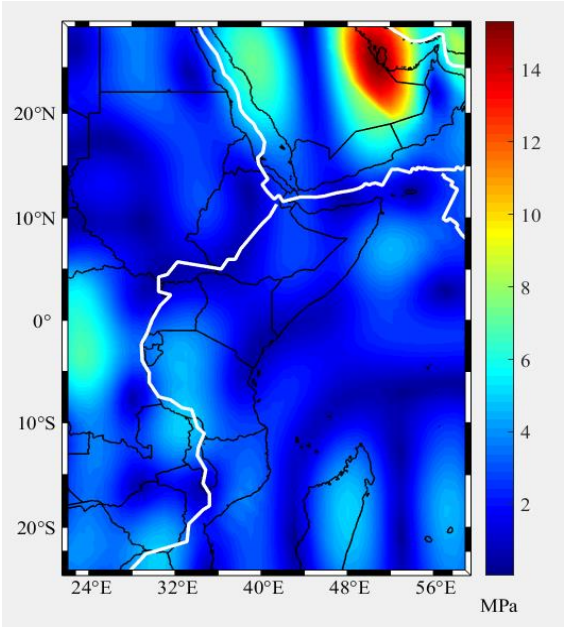

(c)

Figure 8 Lithospheric shear stress at the base of the lithosphere (a) in the east-west direction, (b) in the north-south direction, and (c) the magnitude of the stress

The result in the north-south direction, which is shown in Figure 8(b), implies that most of the estimated north-south component of the shear stress values lies between, the range of -4 MPa and 3 MPa, which is 93.82% of the total pixel values. The high positive values located in the northwest of Saudi Arabia that associate with the normal and strike-slip faulting stress regime where the seismic activity occurred, over the center of the Democratic Republic of Congo, eastern Botswana, and southern Arabian plate (i.e., over the boundary of Yemen and Oman) these locations are

associate with a normal faulting stress regime. The highest negative stress value is located in southwestern Iran (i.e., south of the Eurasian plate) associated with the strike-slip and thrust faulting stress regime. Moreover, the positive stress values are detected along most of the plate boundaries, most of the Arabian plate, most of the Indian Ocean within the African plate, Sudan (i.e., western, central, and southeastern), western Ethiopia, western Kenya, and eastern Egypt. Besides, those positive stress values, the negative stress values are also detected in Figure 8(b) over northern Sudan, southern Egypt, southwest Libya, eastern Central African Republic, northern Democratic Republic of Congo, Zambia, Malawi, Somalia, Madagascar, southern Tanzania, northern Mozambique and some locations in the Indian Ocean within the African plate. In this result, the positive value implies that the stress orientation is towards the north direction and the negative one is towards the south direction. Overall, 55.68% of the resultant horizontal shear stress at the base of the lithosphere throughout the study area is oriented in a northward direction and the remaining 44.32% is oriented in the southward direction. In general, the large positive and negative values of stress (i.e., both in east-west and north-south directions) are characterized by a low lithospheric strength, and contrary to these the small positive and negative values of stress are characterized a stable and rigid lithosphere.

Moreover, the result of the estimated horizontal shear stress magnitude ranges from ≈ 0.04 MPa to ≈ 15.32 MPa as shown in Table 2. As seen in Figure 8(c), the maximum resultant magnitude of lithospheric shear stress is located in eastern Saudi Arabia, Bahrain, and Qatar (i.e., towards the Persian Gulf within the Arabian plate) associated with significant normal faulting stress regimes where seismic events severely occurred. In addition, the minimum one is located in southern Kenya associated with a normal faulting regime of stress, over northwest and southern Sudan which associates with an unknown stress regime as shown on WSM 2016 database, southwest and northern Ethiopia, and some areas around Madagascar over Indian ocean within the Africa plate. Further, the resultant value of lithospheric shear stress magnitude widely lies below 4 MPa, which is 79.18% of the result achieved in the study area. The larger magnitude of horizontal shear stress is associated with a location that is characterized by low lithospheric strength, and those with a smaller magnitude are characterized by a stable and rigid lithosphere layer of the Earth. As the magnitude of the stress increases the lithospheric strength (i.e., being stable and rigid) decreases, and vice versa.

Table 2 Lithospheric shear stress due to mantle convection (Unit: MPa)

	Minimum	Maximum	Mean	STD
$\sigma_{X(EGM08)}$	-14.819517	8.182714	-0.402428	3.170378
$\sigma_{Y(EGM08)}$	-8.103686	3.58602	0.045977	1.808202
$S_{(EGM08)} = \sqrt{(\sigma_{X(EGM08)})^2 + (\sigma_{Y(EGM08)})^2}$	0.03965	15.322646	2.987154	2.13492

The table shows the estimated east-west and north-south statistics of lithospheric shear stress and its magnitude throughout the study area.

4.2 Comparison of the Static Gravity Field Models

The lithospheric shear stress at the base of the lithosphere due to mantle flow from EGM98 and EIGEN-6C4 static gravity field models was computed distinguishably through a gravimetric approach. The result achieved from these static models more or less shows similarity in the horizontal components of shear stress (i.e., shows similarity in east-west and north-south directions) as shown in Figure 9 and Figure 10. However, there is a slight difference between them in both directions, that may be as a consequence of EIGEN-6C4, containing the complete SGG data of the GOCE-Mission. As shown in Figure 9(c), the result in the east-west direction reaches a large positive value difference (i.e., the shear stress in eastward orientation) along the active convergent tectonic margin between the Arabian plate and the Iranian block, or Eurasian plate. This location also associates with the strike-slip and thrust faulting regime, as well as severe seismic events. In addition, the result shows a large negative value difference (i.e., the shear stress has a western orientation) is observed in the eastern part of the Arabian plate towards the Perisian Gulf.

The difference in north-south direction is shown in Figure 10(c), its high positive value (i.e., the shear stress has a northern orientation) in Botswana, the location which is characterized by a thinned lithosphere that has a low lithospheric strength. Further, the large negative values (i.e., the shear stress has a southern orientation) appear over southeastern Saudi Arabia, United Arab Emirates, over the Indian Ocean within the African plate, and the triple junction of EARS (i.e., Afar, northeast of Ethiopia where the seismic events happen frequently and associates with the normal faulting regime). Furthermore, Figure 11(c) depicts the difference in the resultant magnitude of the lithospheric shear stress at the base of the lithosphere, showing the large positive value in southeastern Saudi Arabia and the large negative value in eastern Sudan and southern Malawi.

Table 3 Lithospheric shear stress due to mantle convection using EIGEN-6C4 (Unit: MPa)

	Minimum	Maximum	Mean	STD
$\sigma_{X(EIGEN-6C4)}$	-14.818278	8.181778	-0.40239	3.170159
$\sigma_{Y(EIGEN-6C4)}$	-8.103583	3.586091	0.045992	1.808184
$S_{(EIGEN-6C4)} = \sqrt{(\sigma_{X(EIGEN-6C4)})^2 + (\sigma_{Y(EIGEN-6C4)})^2}$	0.03951	15.32142	2.987028	2.134749

The table shows the estimated east-west and north-south statistics of lithospheric shear stress and its magnitude obtained using EIGEN-6C4 throughout the study area.

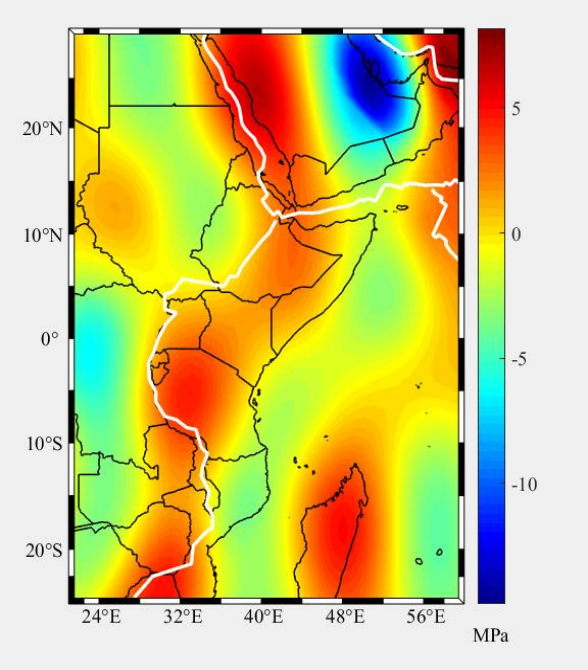

(a)

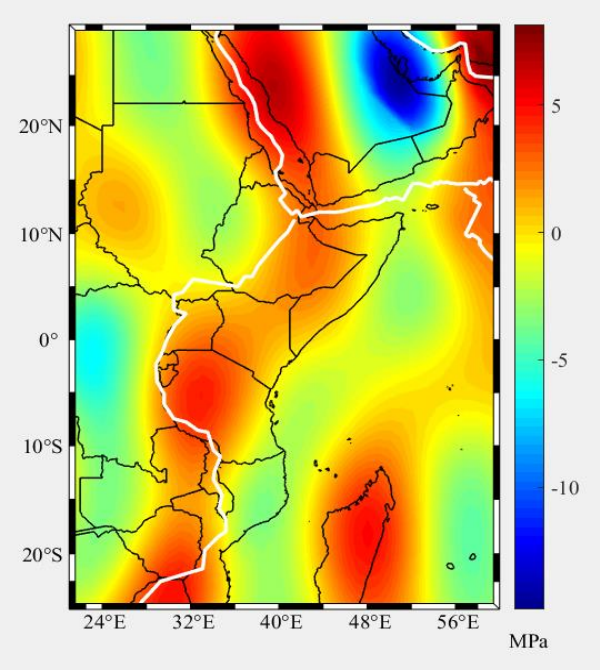

(b)

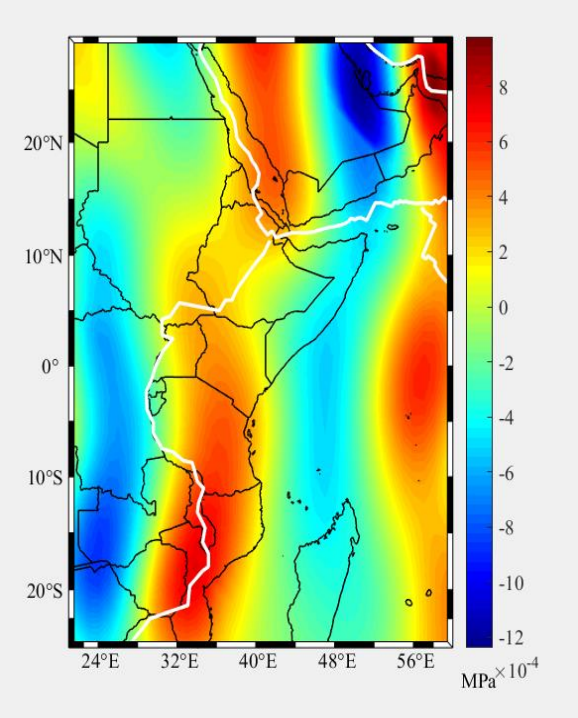

(c)

Figure 9 Horizontal shear stress at the base of the lithosphere in the east-west direction (a) computed using EGM08, (b) computed using EIGEN-6C4, and (c) the difference between the two static gravity field models

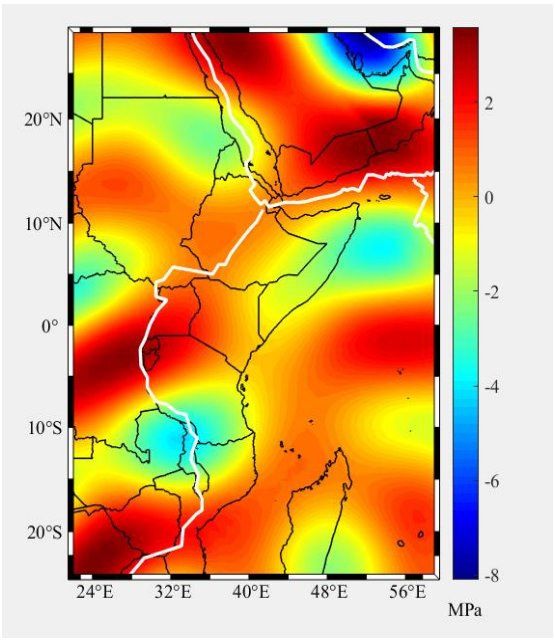

(a)

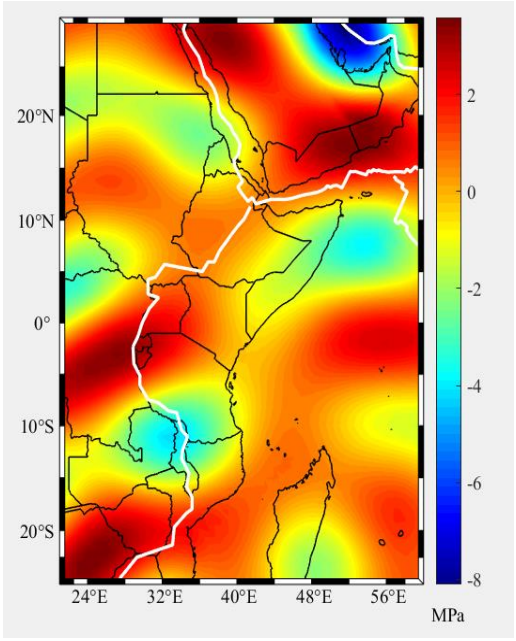

(b)

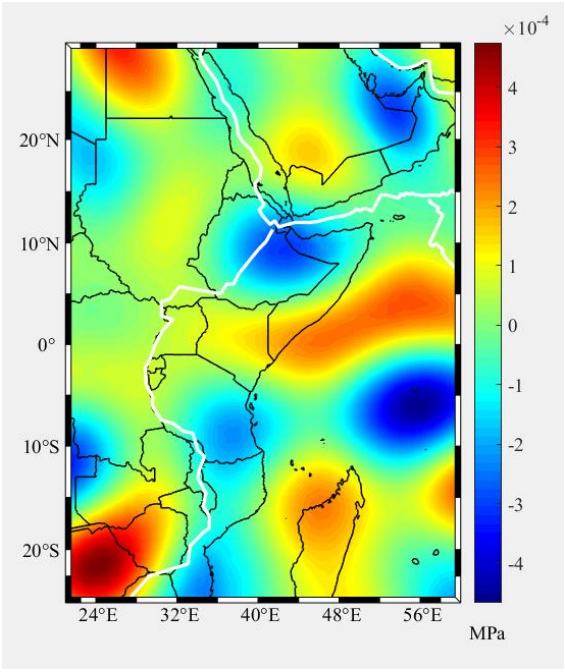

(c)

Figure 10 Horizontal shear stress at the base of the lithosphere in the north-south direction (a) computed using EGM08, (b) computed using EIGEN-6C4, and (c) the difference between the two static gravity field models

.

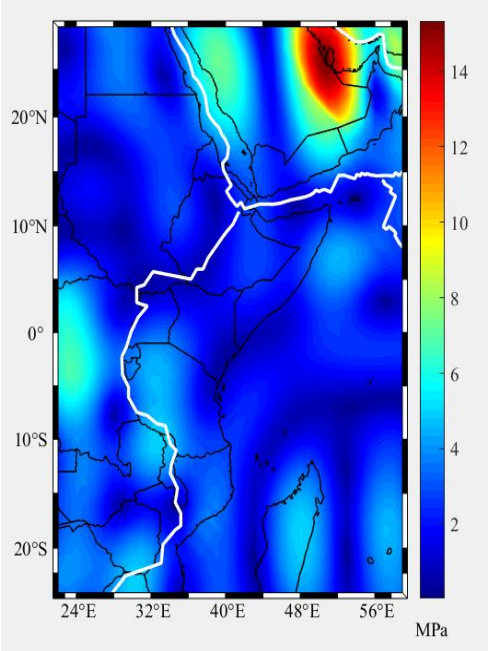

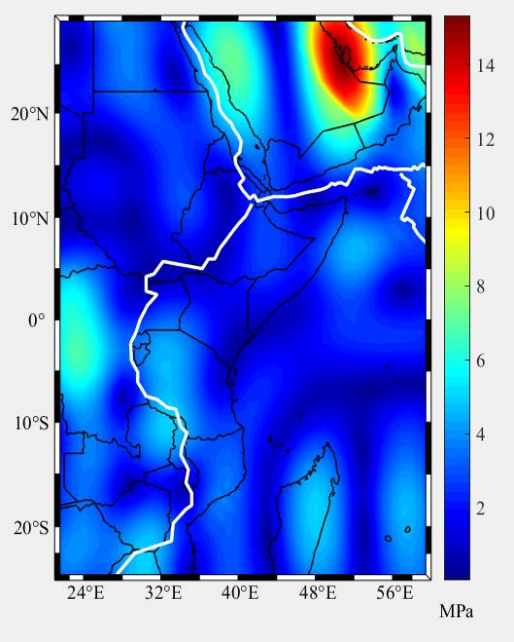

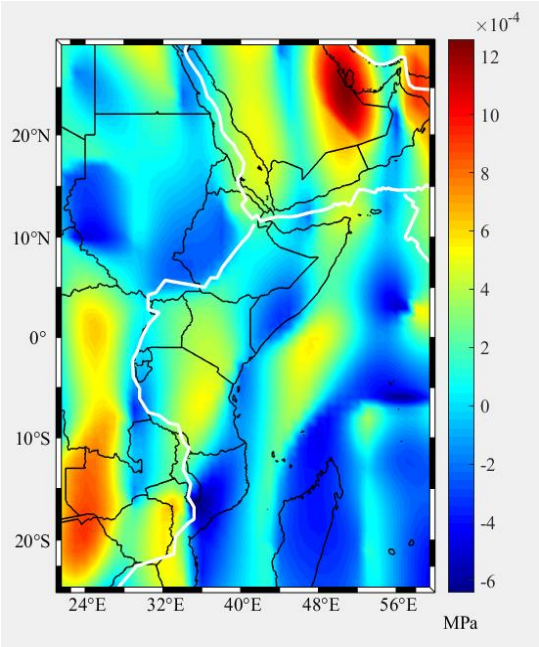

(c)

Figure 11 The resultant magnitude of horizontal shear stress at the base of the lithosphere (a) computed using EGM08, (b) computed using EIGEN-6C4, and (c) the difference between the two static gravity field models

Table 4 Difference in lithospheric shear stress (Unit: MPa)

	Minimum	Maximum	Mean	STD
$\sigma_{X(EGM08)} - \sigma_{X(EIGEN-6C4)}$	-0.001239	0.000984	-0.000036	0.000399
$\sigma_{Y(EGM08)} - \sigma_{Y(EIGEN-6C4)}$	-0.000467	0.000475	0.000005	0.000144
$S_{Diff} = S_{(EGM08)} - S_{(EIGEN-6C4)}$	-0.00065	0.001259	0.000126	0.000326

The table shows the statistics of the difference in the lithospheric shear stress in the east-west and north-south directions as well as the difference in magnitude throughout the study area by using the EGM08 and EIGEN-6C4 static gravity model

4.3 Temporal Variation of Lithospheric Shear Stress

The temporal variation of the stress is assessed by using a GRACE monthly solution of December 2002, 2010, and 2020. The lithospheric shear stress components at the base of the lithosphere are computed based on the method discussed in section 3.3. The result shows that the lithospheric shear stress components at different periods (i.e., in the years 2002, 2010, and 2020), have a similar pattern (i.e., similar orientation), or hardly varied in the east-west and north-south directions. However, the lithospheric shear stress shows a slight variation between the years 2010 and 2002, and also between 2020 and 2002.

Figure 12(c) illustrates the temporal change in the east-west direction between December 2002 and December 2010, the high positive values are located in eastern Zambia and central Saudi Arabia. The high negative value is located along the active convergent tectonic margin between the Arabian plate and the Eurasian plate, where it is characterized by a strike-slip and thrust faulting regime and active seismicity. Further, the variation is significant over Sudan, Egypt, eastern Zambia, west of Zimbabwe, east of Zambia, Malawi, Madagascar, and the southeast border of the study area.

As seen in Figure 13(c) for the temporal change in an east-west direction between December 2002 and December 2020, the location in eastern Zambia, the southeast border of the study area, the eastern border of Kenya towards Uganda and Eritrea (i.e., southwest of Red Sea) exhibit high positive values of variation in lithospheric shear stress. Also, the high negative value is located over southwestern Iran (i.e., the active convergent tectonic margin between the Arabian plate and the Eurasian plate). The variation is significant in the northward orientation of the lithospheric shear stress.

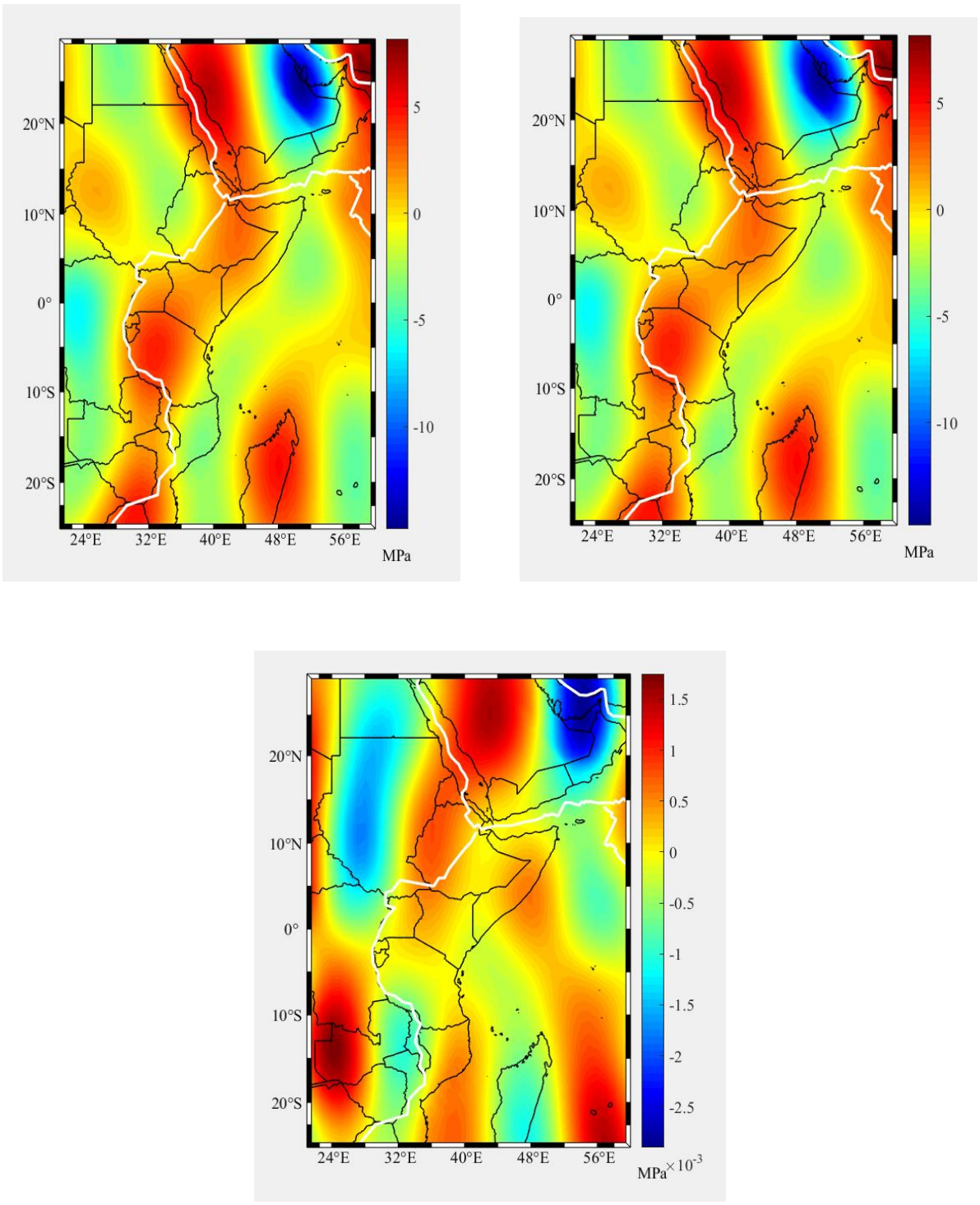

Figure 12 Lithospheric shear stress in east-west direction computed at the base of lithosphere using GRACE monthly solution for (a) December 2002, (b) December 2010, and (c) the variation between 2010 and 2002

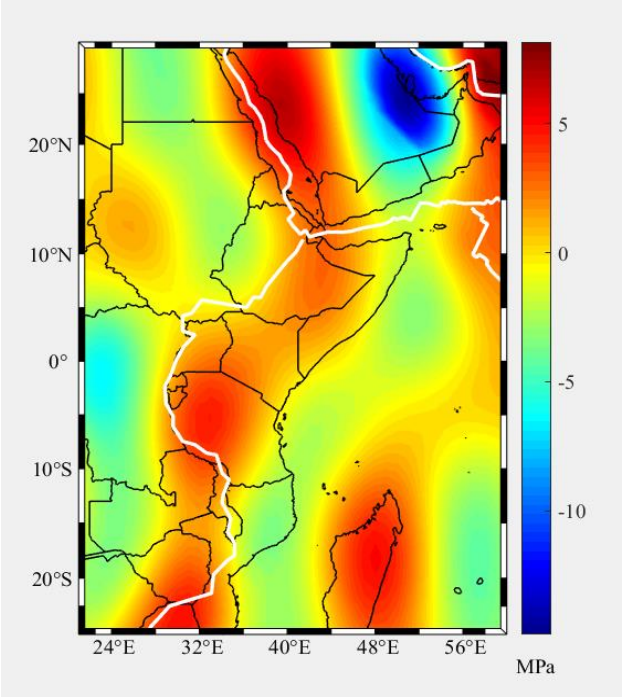

(a)

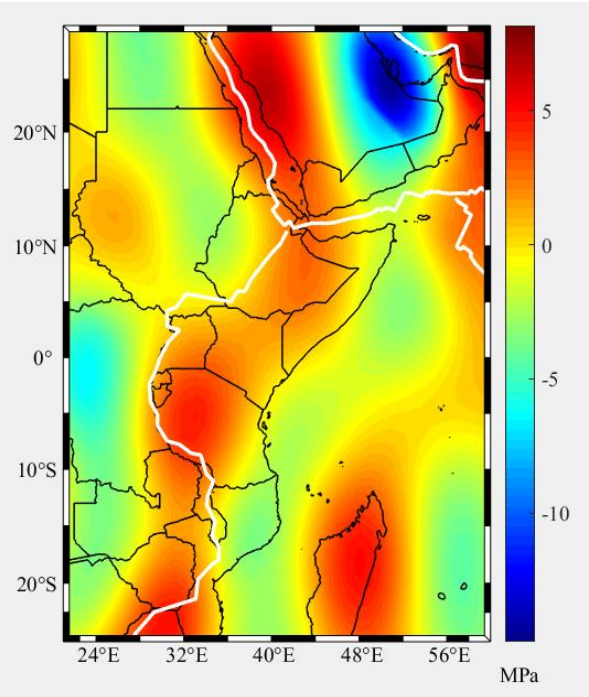

(b)

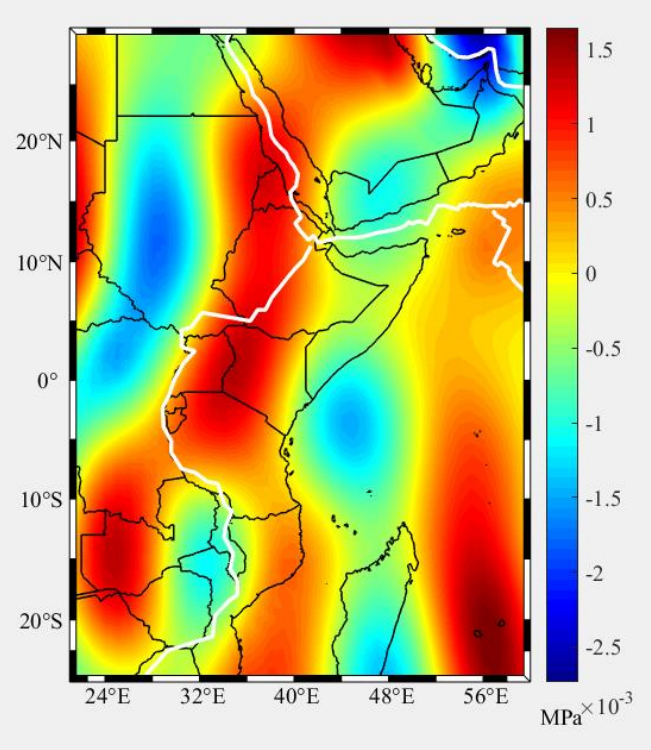

(c)

Figure 13 Lithospheric shear stress in east-west direction computed at the base of lithosphere using GRACE monthly solution for (a) December 2002, (b) December 2020, and (c) the variation between 2020 and 2002

Figure 14(c) depicts a slight variation of shear stress computed at the base of the lithosphere for the December 2002 and December 2010 GRACE monthly solution. The magnitude of the difference achieved in this result implies a small variation than the result achieved in Figure 15(c). The large positive values are seen over the southwestern Democratic Republic of the Congo, eastern Ethiopia (i.e., along the border between Ethiopia and Somalia), eastern Oman, and over the Indian Ocean within the African plate; while the large negative values are located over Botswana. Besides this, Figure 15(c) depicts the variation between December 2002 and December 2020, the large positive values of stress variation are located in the middle of Oman, middle of Democratic Republic of Congo, central Mozambique, a place over the Indian Ocean and the middle of Red Sea. Whereas, the large negative value is located over the southeastern Central African Republic, South of Somalia, and Botswana.

Table 5 Lithospheric shear stress due to mantle convection using GRACE (Unit: MPa)

	Minimum	Maximum	Mean	STD
$\sigma_{X(2002)}$	-14.817528	8.182723	-0.40235	3.170113
$\sigma_{Y(2002)}$	-8.103312	3.586143	0.04602	1.808182
$\sigma_{X(2010)}$	-14.819132	8.181535	-0.40239	3.170167
$\sigma_{Y(2010)}$	-8.103848	3.586309	0.045984	1.808209
$\sigma_{X(2020)}$	-14.817722	8.180942	-0.40234	3.170115
$\sigma_{Y(2020)}$	-8.104234	3.586283	0.045974	1.808311
$S_{(2002)}$	0.039882	15.32071	2.987018	2.134687
$S_{(2010)}$	0.039779	15.32237	2.986992	2.134832
$S_{(2020)}$	0.039531	15.32095	2.987088	2.134698

Table 5 show the statistics of the lithospheric shear stress in the east-west and north-south directions as well as the magnitude throughout the study area by using the GRACE monthly solution of the year 2002, 2010, and 2020.

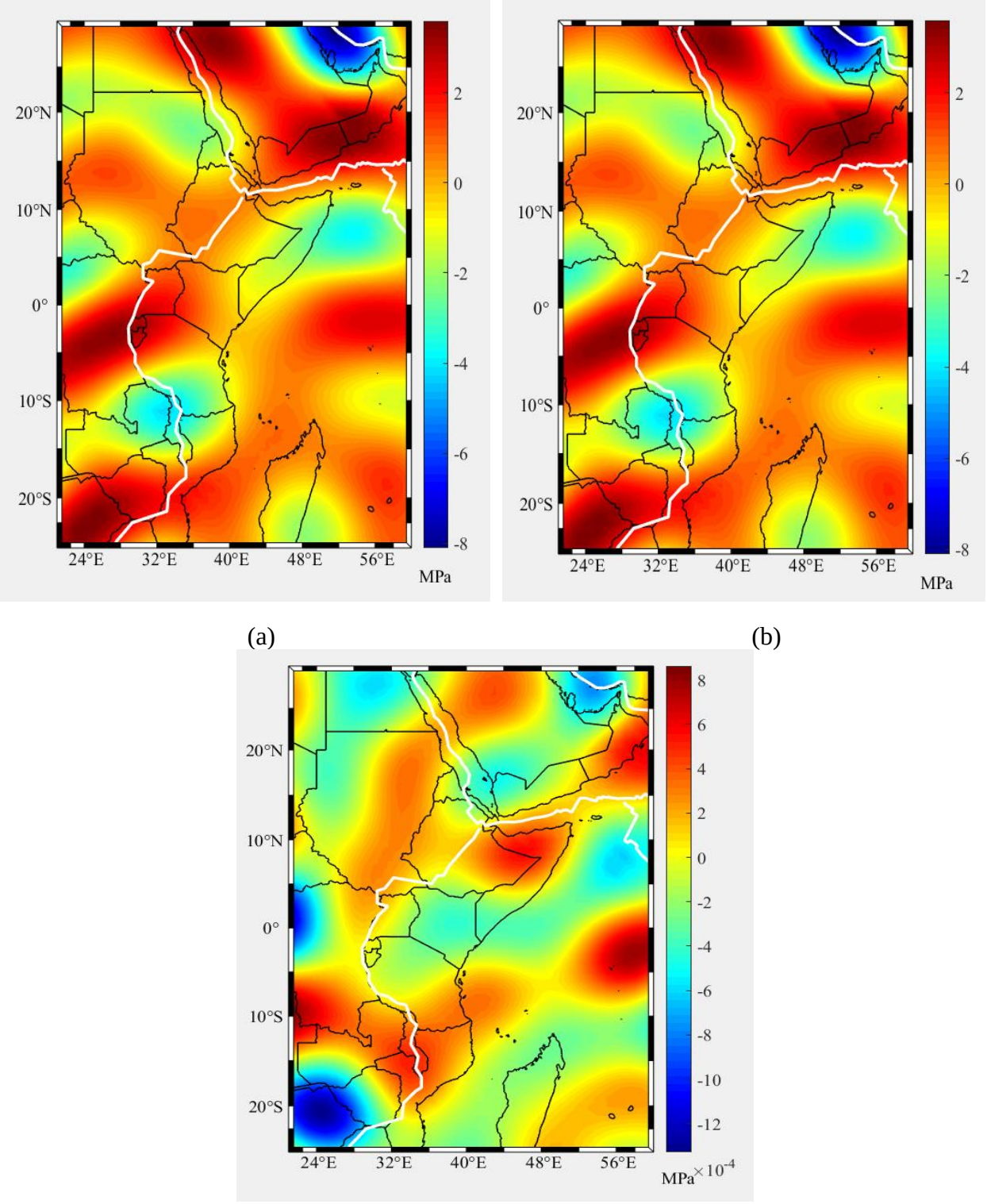

Figure 14 Lithospheric shear stress in north-south direction computed at the base of lithosphere using GRACE monthly solution for (a) December 2002, (b) December 2010, and (c) the variation between 2010 and 2002

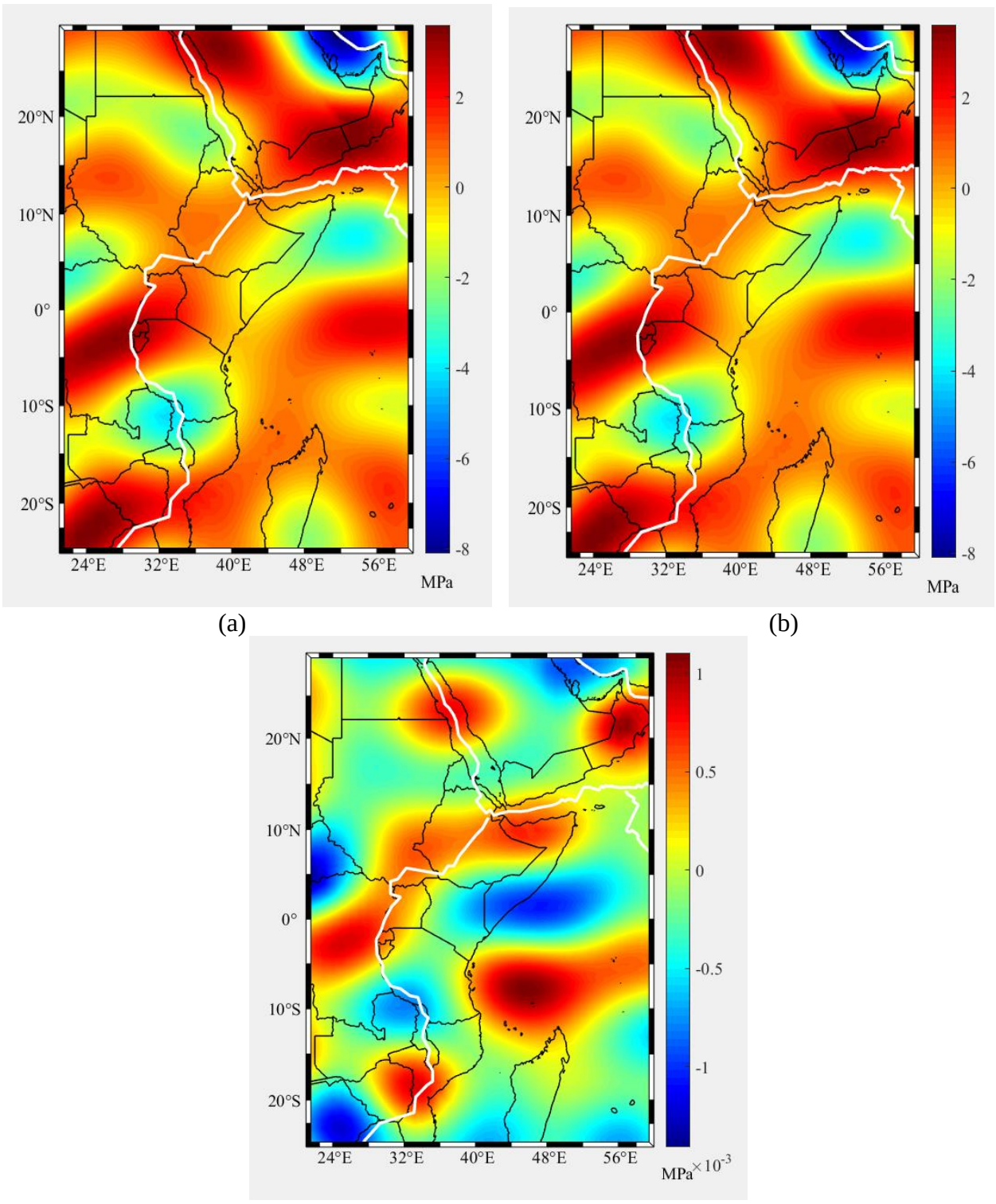

Figure 15 Lithospheric shear stress in north-south direction computed at the base of lithosphere using GRACE monthly solution for (a) December 2002, (b) December 2020, and (c) the variation between 2020 and 2002

Table 6 The variation in lithospheric shear stress due to mantle convection (Unit: MPa)

	Minimum	Maximum	Mean	STD
$\sigma_{X(2010)} - \sigma_{X(2002)}$	-0.002899	0.001751	-0.000039	0.000792
$\sigma_{Y(2010)} - \sigma_{Y(2002)}$	-0.001329	0.000865	-0.000035	0.000335
$\sigma_{X(2020)} - \sigma_{X(2002)}$	-0.002737	0.001644	0.000005	0.000781
$\sigma_{Y(2020)} - \sigma_{Y(2002)}$	-0.001408	0.001106	-0.000046	0.00045
$S_{VARI} = S_{(2010)} - S_{(2002)}$	-0.00174	0.002809	-0.000025	0.000693
$S_{VARI} = S_{(2020)} - S_{(2002)}$	-0.00219	0.001578	0.00007	0.000693

Table 6 show the statistics of the lithospheric shear stress temporal variation in the east-west and north-south directions as well as the magnitude throughout the study area by using the GRACE monthly solution between the year 2002 and 2010; and between 2002 and 2020.

CHAPTER FIVE

5. Discussion

The overall objective of the study was the evaluation of the horizontal shear stress and the temporal variation due to mantle convection at the base of the lithosphere via a gravimetric approach. The study evaluates the lithospheric shear stress using a static gravity field, assesses the temporal variation of stress using GRACE monthly data solution, and performs a comparison of static gravity field models.

The static gravity field data with some information about topographic height, crustal thickness, and lithospheric thickness were used in this study. As a result, more geophysical information and data are applied for the computation of stress in this approach. The model recovered through this approach shows the spatial pattern of lithospheric shear stress, (i.e., the high, low, and moderate value of stress as well as the orientation of stress), as shown in the result section.

This study applied the Runcorn stress equations and higher degree ($13 \leq n \leq 25°$) harmonic coefficients of geopotential to compute horizontal shear stress exerted by mantle convection at the base of the lithosphere. The results in the east-west and north-south directions revealed that stresses computed in this study more or less show good agreement with the location of seismic events obtained from ISC as depicted in Figure 6, and the WSM 2016 (i.e., the direction of maximum horizontal shear stress, the stress regimes, and the absolute plate motion). The stress increases towards the area where active seismicity occurred (i.e., the lithospheric strength becomes low or the area that has thinned lithosphere), in contrary the stress decreases towards the location characterized by strong lithospheric strength (stable and rigid lithosphere) where the seismic events hardly happened. The lithospheric shear stress thus derived exerted by mantle convection at the base of the lithosphere agrees well with the mantle flow pattern in the region of EARS (Liu, 1977), and is consistent with the geological facts and geophysical theories about the East African Rift System and the African tectonic structure (Ring, 2014).

The result obtained from two different gravity field models shows similar orientations of lithospheric shear stress components. The stress obtained as a result of using EGM08 shows a maximum value of 14.819517 MPa in westward orientation and 8.182714 MPa in eastward orientation, as well as a minimum value of 0.03965 MPa and maximum value of 15.322646 MPa of the overall resultant magnitude of stress. Also, the maximum value of stress is 8.103686 MPa and 3.58602 MPa in southward and northward orientation respectively. Moreover, the stress obtained from EIGEN-6C4 has a maximum value of 14.818278 MPa in westward and 8.181778 MPa in eastward orientation as well as a maximum value of 8.103583 MPa and 3.586091 MPa.in the south and north orientation of the lithospheric shear stress respectively. Also, it has a minimum value of 0.03951 MPa and a maximum value of 15.32142 MPa of the resultant magnitude of stress.

As a result, there is no marked difference (i.e., there is a good consistency between the result obtained using EGM08 data sets versus EIGEN-C64 data sets), apart from a slight difference as shown in section 4.2. The result depicts a maximum value of difference 0.001239 MPa and 0.000984 MPa in westward and eastward orientation. Also, a maximum of 0.000467 MPa and

0.000475 MPa difference is shown in southward and northward orientation. Further, the two static gravity field models have a slight difference in their resultant magnitude too (i.e., a maximum value of 0.001259 MPa and a minimum value of -0.00065 MPa lithospheric shear stress magnitude).

The lithospheric shear stress components were assessed at a different period using GRACE monthly data solution, and exhibit relatively the same pattern of orientation, even though it shows a slight change within the study area as illustrated in section 4.3. The stress shows a maximum value of 14.817528 MPa, 14.819132 MPa, and 14.817722 MPa in the westward orientation, and 8.182123 MPa, 8.181535 MPa, and 8.180942 MPa of stress for the year 2002, 2010 and 2020 respectively. The maximum variation in westward orientation is about 0.002899 MPa and 0.002737 MPa, as well as 0.001751 MPa and 0.001644 MPa in eastward orientation for the year between December 2010 and December 2002 and for the year between December 2020 and December 2002. On the other hand, the maximum variation of stress about 0.001329 MPa and 0.001408 MPa in southward, as well as 0.000865 MPa and 0.001106 MPa in northward orientation are exhibited for the year between December 2010 and December 2002 and the year between December 2020 and December 2002.

In general, the result obtained through the gravimetric approach using a static gravity field and the temporal variation assessed using GRACE monthly solution is consistent with the WSM2016 database and the seismic events in the study area.

CHAPTER SIX

6. Conclusion and Recommendation

6.1 Conclusion

The gravimetric approach by using a static gravity field and GRACE/GRACE-FO monthly solution was carried out to evaluate the static lithospheric shear stress and its temporal change in the East African Great Rift Valley due to mantle flow in the lithosphere. Extracting sub-surface information from gravity measurements is a fundamental task. Since the Earth's gravity field is a reflection of its internal structure, changes in the gravity field also affect the lithospheric stress that is transmitted throughout the lithosphere. Some geophysical information was added for better determination and understanding of the causal relationship between mantle convection and lithospheric stress based on the measured gravimetric quantity. Therefore, this method is different than the purely gravimetric one.

The method presented in this study for lithospheric shear stress evaluation as well as to assess the temporal variation of stress is based on Runcorn's solution which is the direct way to connect the mantle convection to the Earth's gravity field. This study used a short wavelength portion of gravity field between degrees 13 and 25 by considering the lithospheric shear stress induced by mantle convection, and the GRACE/GRACE-FO monthly data solution of December 2002, 2010, and 2020 within the same degrees of harmonic coefficient of geopotential to compute static shear stress and its temporal variation.

The study applied two different static gravity field models with the same methodology, to detect changes in stress, and the result shows a minor change. The same wise the result results of the temporal variation show a minor change in the lithospheric shear stress components. The result obtained by using EGM08 static gravity model is consistent with the WSM2016 and seismic events provided by ISC. Further, based on the analysis of results of gravimetric approach stress determination, the computed lithospheric shear stress integrated with mantel flow pattern, the geological facts and geophysical theories about the East African Rift System and the African tectonic structure.

6.2 Recommendation

This study is recommended for the geosciences that need vital information about the state of horizontal stress and its temporal variation using a static gravity field and GRACE data over a wide geographic area, that incorporates the East African Great Rift Valley, which is the major and most active continental rift system in the world. The study is appropriate for places which are lacking gravimetric and seismic data; hence it gives good coverage of the entire area using satellite gravity missions.

Even though geophysical information is incorporated in this study, in addition to the gravimetric datasets, it is recommended that future research shall consider more geophysical information to achieve a better result. Also, the study compares the results of the lithospheric shear stresses obtained from two distinct static gravity models. Future studies shall compromise various models in this study area.

Further, it is recommended to use a full wavelength portion of the gravity field for better investigation of the lithospheric shear stress induced by mantle convection, and the consecutive GRACE/GRACE-FO monthly data solution of long periods to compute static shear stress and assess the temporal variation of stress.

Bibliography

Bagherbandi, M. (2011). *An Isostatic Earth Crustal Model and Its Applications* (Issue April).

Bettadpur, S. (2003). Gravity Recovery and Climate Experiment, Level-2 Gravity Field Product User Handbook. *Center for Space Research ,The University of Texas at Austin*, *734*.

Boergens, E., Andreas, G., Dobslaw, H., & Dahle, C. (2020). Quantifying the Central European Droughts in 2018 and 2019 with GRACE-Follow-On. *Geophysical Research Letters 13*, 1–20. https://doi.org/10.1029/2020GL087285

Chen, J. (2018). Satellite gravimetry and mass transport in the earth system. *Geodesy and Geodynamics*, *245*, 1–14. https://doi.org/10.1016/j.geog.2018.07.001

Chorowicz, J. (2005). The East African rift system. *Journal of African Earth Sciences*, *43*, 379–410. https://doi.org/10.1016/j.jafrearsci.2005.07.019

Conrad, C. P., & Lithgow-bertelloni, C. (2006). Influence of continental roots and asthenosphere on plate-mantle coupling. *GEOPHYSICAL RESEARCH LETTERS*, *33*(January), 2–5. https://doi.org/10.1029/2005GL025621

Cooley, S. S., & Landerer, F. W. (2020). Gravity Recovery and Climate Follow-on (GRACE-FO), Experiment Level-3 Data Product User Handbook. *Jet Propulsion Laboratory,California Institute of Technology*, 1–58.

Corti, G. (2012). Tectonophysics Evolution and characteristics of continental rifting : Analog modeling-inspired view and comparison with examples from the East African Rift System. *Tectonophysics*, *522–523*, 1–33. https://doi.org/10.1016/j.tecto.2011.06.010

Eakins, B. W., & Division, G. (2009). ETOPO1 1 ARC-MINUTE GLOBAL RELIEF MODEL: PROCEDURES, DATA SOURCES AND ANALYSIS. *NATIONAL OCEANIC AND ATMOSPHERIC ADMINISTRATIO*.

Ebinger, C. J., Bechtel, T. D., Forsyth, D. W., & Bow, C. O. (1989). Effective Elastic Plate Thickness Beneath the East African and Afar Plateaus and Dynamic Compensation of the Uplifts. *JOURNAL OF GEOPHYSICAL RESEARCH*, *94*, 2883–2901.

Eshagh, M. (2010). Acta Geophysica Alternative Expressions for Gravity Gradients in Local North-Oriented Frame and Tensor Spherical Harmonics. *GEOPHYSICAL RESEARCH LETTERS*, *58*(2), 215–243. https://doi.org/10.2478/s11600-009-0048-z

Eshagh, M. (2014). From Satellite Gradiometry Data to Subcrustal Stress Due to Mantle Convection. *Pure and Applied Geophysics*, *171*, 2391–2406. https://doi.org/10.1007/s00024-014-0847-2

Eshagh, M. (2015). On the relation between Moho and sub-crustal stress induced by mantle convection. *Journal of Geophysics and Engineering*, *12*, 1–11. https://doi.org/10.1088/1742-2132/12/1/1

Eshagh, M. (2017). Local recovery of lithospheric stress tensor from GOCE gravitational tensor. *Geophysical Journal International*, *209*, 317–333. https://doi.org/10.1093/gji/ggx026

Eshagh, M. (2021). *SATELLITE GRAVIMETRY AND THE SOLID EARTH Mathematical*

Foundations. https://doi.org/10.1016/B978-0-12-816936-0.01001-X

Eshagh, M., Fatolazadeh, F., & Tenzer, R. (2020). Lithospheric stress , strain and displacement changes from GRACE-FO time-variable gravity : case study for Sar-e-Pol Zahab Earthquake 2018. *Geophys. J. Int.*, *223*, 379–397. https://doi.org/10.1093/gji/ggaa313

Eshagh, M., Hussain, M., & Tiampo, K. F. (2016). Towards sub-lithospheric stress determination from seismic Moho, topographic heights and GOCE data. *Journal of Asian Earth Sciences*, 1–44. https://doi.org/10.1016/j.jseaes.2016.07.024

Eshagh, M., & Romeshkani, M. (2015). Determination of sub-lithospheric stress due to mantle convection using GOCE gradiometric data over Iran. *Journal of Applied Geophysics*, 1–17. https://doi.org/10.1016/j.jappgeo.2015.08.001

Eshagh, M., & Tenzer, R. (2015). Sub-crustal stress determined using gravity and crust structure models. *Comput Geosci*, *19*, 115–125. https://doi.org/10.1007/s10596-014-9460-9

Förste, C., Bruinsma, S. L., Abrikosov, O., Lemoine, J.-M., Schaller, T., Götze, H.-J., Ebbing, J., Marty, J. C., Flechtner, F., Balmino, G., & Biancale, R. (2014). *EIGEN-6C4 The latest combined global gravity field model including GOCE data up to degree and order 2190 of*.

Fu, R., & Huang, P. (1983). The global stress field in the lithosphere obtained from the satellite gravitational harmonics. *Physics Ofthe Earth and Planetary Interiors*, *31*, 269–276.

Gido, N. A. A., Bagherbandi, M., & Sjöberg, L. E. (2018). A gravimetric method to determine horizontal stress field due to flow in the mantle in Fennoscandia. *Geosciences Journal*.

Han, S., Shum, C. K., Jekeli, C., Kuo, C., Wilson, C., & Seo, K. (2005). Non-isotropic filtering of GRACE temporal gravity for geophysical signal enhancement. *Geophys. J. Int.*, *163*, 18–25. https://doi.org/10.1111/j.1365-246X.2005.02756.x

Heidbach, O., Mojtaba Rajabi, M., Reiter, K., & Ziegler, M. (2016). World Stress Map 2016. *GFZ Data Service*. https://doi.org/10.5880/WSM.2016.001.0

Hofmann-wellenhof, B., & Moritz, H. (2005). *Physical Geodesy*.

Huang, P., & Fu, R. (1982). The mantle convection pattern and force source mechanism of recent tectonic movement in China. *Physics Ofthe Earth and Planetary Interiors*, *28*, 261–268.

Ince, E. S., Barthelmes, F., Reißland, S., Elger, K., & Förste, C. (2019). ICGEM – 15 years of successful collection and distribution of global gravitational models , associated services , and future plans. *Earth System Sciience Data*, *11*, 647–674.

Kusche, J., Schmidt, R., Petrovic, S., & Rietbroek, R. (2009). Decorrelated GRACE time-variable gravity solutions by GFZ, and their validation using a hydrological model. *Journal of Geodesy*, *83*(10), 903–913. https://doi.org/10.1007/s00190-009-0308-3

Landerer, F. W., Flechtner, F. M., Save, H., Webb, F. H., Bandikova, T., Bertiger, W. I., Bettadpur, V., Byun, S., Dobslaw, H., Fahnestock, E., Loomis, B. D., Murböck, M., Wiese, D. ., Dahle, C., Harvey, N., Kang, Z., Kruizinga, L. H., Loomis, B. D., Mccullough, C., … Yuan, D.-N. (2020). Extending the global mass change data record : GRACE Follow-On

instrument and science data performance. *Geophysical Research Letters*. https://doi.org/10.1029/2020GL088306

Laske, G., Masters, G., Ma, Z., & Pasyanos, M. (2013). Update on CRUST1.0 - A 1-degree Global Model of Earth ’s Crust. *Geophysical Research*, *15*, 2658.

Lithgow-bertelloni, C., & Guynn, J. H. (2004). Origin of the lithospheric stress field. *JOURNAL OF GEOPHYSICAL RESEARCH*, *109*(August 2003), 1–32. https://doi.org/10.1029/2003JB002467

Liu, H. (1977). Convection pattern and stress system under the african plate. *Physics Ofthe Earth and Planetary Interiors*, *15*, 60–68.

Liu, H. (1978). MANTLE CONVECTIONPATTERN AND SUBCRUSTAL STRESS FIELD UNDER ASIA. *Physics Ofthe Earth and Planetary Interiors*, *16*, 247–256.

Liu, H. (1979). CONVECTION-GENERATED STRESS CONCENTRATION AND SEISMOGENIC MODELS OF THE TANGSHAN EARTHQUAKE. *Physics of the Earth and Hanetary Interiors*, *19*, 307–318.

McNutt, M. (1980). Implications of Regional Gravity for State Stress in the Earth’s Crust and Upper Mantle. *JOURNAL OF GEOPHYSICAL RESEARCH*, *85*, 6377–6396.

Moritz, H. (1990). The inverse Vening Meinesz problem in isostasy. *Geophysical Journal International*, *102*, 733–738.

Morley, C. K., Ngenoh, D. K., & Ego, J. K. (1999). Introduction to the East African Rift System. *Geoscience of Rift Systems—Evolution of East Africa: AAPG Studies in Geology*, *44*, 1–18.

Pavlis, N. K., Holmes, S. A., Kenyon, S. C., & Factor, J. K. (2012). The development and evaluation of the Earth Gravitational Model 2008 (EGM2008). *GEOPHYSICAL RESEARCH*, *117*(April), 1–38. https://doi.org/10.1029/2011JB008916

Prevost, P., Chanard, K., Fleitout, L., Calais, E., Walwer, D., Prevost, P., Chanard, K., Fleitout, L., Calais, E., Walwer, D., Prevost, P., Chanard, K., Fleitout, L., Calais, E., Walwer, D., Dam, T. Van, & Ghil, M. (2019). Data-adaptive spatio-temporal filtering of GRACE data. *Geophysical Journal International*, *219*, 2034–2055. https://doi.org/10.1093/gji/ggz409

Ricard, Y., Fleitout, L., & Froidevaux, C. (1984). Geod heights and lithospheric stresses for a dynamic Earth. *Annales Geophysicae*, *2*, 267–286.

Ring, U. (2014). The East African Rift System. *Austrian Journal of Earth Sciences*, *107*, 132–146.

Runcorn, S. K. (1964). Satellite Gravity Measurements and a Laminar Viscous Flow. *JOURNAL OF GEOPHYSICAL RESEARCH*, *69*(20).

Runcorn, S. K. (1967). Flow in the Mantle Inferred from the Low Degree Harmonics of the Geopotential. *Geophys. J. R. Astr. SOC*, *14*, 375–384.

Save, H. (2019). Gravity Recovery and Climate Experiment Follow-On CSR Level-2 Processing Standards Document For Level-2 Product Release 06. *Center for Space Research , The University of Texas at Austin*, *01*.

Schmidt, R., Flechtner, F., Meyer, U., Neumayer, K.-H., Dahle, C., Ko¨nig, R., & Kusche, J. (2008). Hydrological Signals Observed by the GRACE Satellites. *Surv Geophys*, *29*, 319–334. https://doi.org/10.1007/s10712-008-9033-3

Seeber, G. (2003). *Satellite Geodesy*.

Sjöberg, L. E. (2009). Solving Vening Meinesz-Moritz inverse problem in isostasy. *Geophys. J. Int.*, *179*, 1527–1536. https://doi.org/10.1111/j.1365-246X.2009.04397.x

Sjöberg, L. E. (2013). On the isostatic gravity anomaly and disturbance and their applications to Vening Meinesz – Moritz gravimetric inverse problem. *Geophys. J. Int.*, *193*, 1277–1282. https://doi.org/10.1093/gji/ggt008

Sjöberg, L. E., Agherbandi, M., & Tenzer, R. (2015). On Gravity Inversion by No-Topography and Rigorous Isostatic Gravity Anomalies. *Pure and Applied Geophysics*, *172*, 2669–2680. https://doi.org/10.1007/s00024-015-1032-y

Sjöberg, L. E., & Bagherbandi, M. (2017). *Gravity Inversion and Integration*.

Torge, W., & Müller, J. (2012). *Geodesy*.

Vening-Meinesz, F. A. (1931). UNE NOUVELLE METHOBE POUR LA REDUCTION ISOSTATIQUE REGIONALE DE L'INTENSITI~ DE LA PESANTEUR'. *GEODIESIQUE*.

Vermeer, M. (2020). *PHYSICAL GEODESY*. Aalto University.

Zoback, M. D., & Zoback, M. Lou. (2002). Stress in the Earth's Litosphere. *Encyclopedia of Science and Technology*, *16*.

Zoback, M. L., & Zoback, M. (1980). State of Stress in the Conterminous United States the San of the San. *Journal of Geophysical Research*, *85*, 6113–6156.

Zoback, M. L., & Zoback, M. (2009). Lithosphere Stress and Deformation. *Elsevier B.V.*, 253–273.